A group-theoretical treatment of approximate symmetry elevation towards bulk symmetry in semiconducting nanocrystals

Author CID:
01881584

Supervisor:
Prof Dimitri D. Vvedensky

Assessor:
Dr Paul Tangney

Word count:
9,850

Date: April 27, 2024

"Hidden Symmetries, or, The Crystal's Inside is What Counts"

A major goal of Physics is making predictions. What sets Physics apart from esoterism is the *scientific method*–a theory that disagrees with empirical evidence cannot reliably produce correct predictions, and hence it has little value as a description of Nature. The uphill battle physicists wage is that against the complexity of Nature, since rigorous theories are difficult to apply to real-world situations. However, sometimes it is possible to take a mathematical shortcut and describe a complex system by simple, fundamental properties, which allows us to make predictions without understanding all the inner dynamics present. This is why symmetry is a physicist's best friend.

Studying quantum mechanics often boils down to solving the Schrödinger equation, which describes a system through its energy. This is usually hard, but imagine a situation where altering the equation in some way leaves it unchanged. For instance, if I stand on an atomic nucleus and then walk to a different point on its surface, essentially rotating the whole picture, I should not be able to tell the difference. Now, if a solution to the corresponding Schrödinger equation remains unchanged when similarly rotated, you would not be surprised. But if it *does* change, the new object should also be a solution to the equation– and even one corresponding to the same energy! Et voilà, that is the power of symmetries.

Quantum dots are tiny crystals, with many applications in medicine, engineering, quantum computing, and others. This is (partly) because they emit light in a tunable, predictable manner–that is why they used to be called "artificial atoms". Predicting how crystals emit light is difficult, but because quantum dots have regular shapes, we can tell a lot about their light spectra based only on their symmetries. This is because the kind of light emission we are interested in is governed by the electrons living around the atoms in the crystal, which interact in a such a way that their energies depend on how they behave when rotated.

If we ignore the crystal shape, electrons close to atom nuclei see a world with full rotation symmetry. When we state the shape of the crystal, only certain rotations remain symmetries– others now affect the Schrödinger equation, messing up the solutions. This means that a pair of solutions we were able to freely transform into one another before may now become separated if the crystal shape forbids all rotations that served this mutual transformation. Now, the solutions will still (with ragged edges) be proper solutions, but their energies will be different, and the energy splitting will show in the spectrum. Knowing the crystal shape means we can predict these kinks in the spectrum, seen as a number of tightly-spaced lines.

In 2015, several papers were published about an apparent failure of this whole idea. Quantum dots grown in the shape of triangular pyramids sometimes behave as if their shape was a triangular prism. Now, forbidding symmetries which would otherwise be present– "symmetry breaking"–is normal and can be caused by many effects which add detail to the picture, but here it seems that these crystals *gain* symmetries. And no one knows why.

Suspiciously, the inside of a crystal consists of a lattice of atoms, and as such, it also has an associated symmetry of rotations which keep the lattice unchanged. This "bulk symmetry" limits the *true* symmetry of the whole system. Now, for our crystal this bulk symmetry is that of a regular tetrahedron, higher than the symmetry of the crystal shape. If the shape of the crystal is just *slightly* different from a shape which actually has this higher symmetry, then Schrödinger solutions which are tiny around the crystal edges will *approximately* resemble other solutions when rotated by these extra rotations provided by the lattice. We tested the predictions the bulk symmetry gives, and there seems to be partial agreement!

Sadly, the measurements show that quantum dots are labile and their spectra may change between samples. Even the qualitative things–number of lines–are difficult to predict. So while our theory sometimes disagrees with experiment, it is not useless; moving towards agreement shows a step in the right direction. And sometimes, that step is another symmetry.

1   Abstract

We investigate the photoluminiscence spectra of InGaAs pyramidal quantum dots with a triangular base under exciton decay. We employ an envelope-function treatment for the exciton wavefunctions, deriving the envelope effective Hamiltonian at the Γ point (point of zero crystal momentum, which in nanocrystals corresponds to envelope functions being in the ground state). We review the principles of arguments based on Hamiltonian symmetries in group-theory formalism, specifically the predictions they provide for energy level degeneracies and the selection rules for transitions induced by weak perturbation. We review the claim made by Karlsson *et al.* (2015) that pyramidal quantum dots with triangular base (symmetry group C_{3v}) exhibit laser-induced photoluminiscence spectra characteristic of structures with a higher symmetry (symmetry group D_{3h}). We propose a theoretical model based on first-order perturbations to symmetry selection rules as a possible mechanism for symmetry elevation, and the condition of localisation within the quantum dot bulk which the model imposes on the wavefunction of an exciton that undergoes symmetry elevation. We claim that exciton complexes with equal charge and equal number of electrons are more likely to undergo symmetry elevation when they are dominated by heavy holes. Because the crystal lattice in the quantum dot restricts the true Hamiltonian symmetries, we claim that D_{3h} is not a candidate of the elevated symmetry group within our model, and we identify T_d as the only possible candidate symmetry group if no *a priori* symmetry breaking is postulated, because it is the bulk symmetry. We compare the predictions T_d yields to both the data measured by Karlsson *et al.* and a new dataset provided by our colleagues, finding good agreement for a part of the studied sample for several exciton complexes. We conclude that either some exciton complexes elevate to the bulk symmetry or the experiments mistakenly identify non-zero z-polarised components in multiple emission lines. We review the condition of raising valence band degeneracy at Γ which elevating to T_d requires, and which is not treated within our proposed model. We discuss further analysis of elevation to bulk symmetry in nanocrystals, as well as the exciton transformation properties disregarded in our simplistic model.

2 Contents

3 Introduction

Quantum dots (QDs) have been the subject of keen interest and study by the scientific community in the last decades for their wide applications in quantum information [1, 2], photonics [3, 4], medicine [5, 6], and many others [7]. Many of these applications are viable due to the unique electronic properties of QDs that allow us to construct within it atom-like electron states [8] with tunable energy levels [9] which depend on the specific manufacturing parameters. However, there are still challenges in characterising the small-scale structural properties of grown QDs, such as unintentional symmetry breaking [10]. In the project, we inspect these structural properties using spectroscopy and the mathematical toolset of group theory.

Quantum dots are semiconductor nanocrystals [7] which enjoy programmable charge states of electrons and electron holes (together dubbed exciton complexes) [11]. The most direct way to experimentally investigate the energy states of electrons and electron holes in QDs is photoluminiscence spectroscopy, a technique used by Karlsson *et al.* [10]. The QDs are first non-resonantly excited by a laser and then spontaneously emit photons due to state transitions of exciton complexes. Each exciton complex may correspond to multiple tightly-spaced energy levels. Determining these energy levels, as well as the selection rules that rule which transitions between them are allowed, is then sufficient to describe the QD spectrum.

The energy level splitting for exciton complexes can be investigated by first considering the exciton as a state of multiple fermionic particles which couple their total angular momenta, and then inserting these eigenstates of total angular momentum into the structure of the quantum dot, breaking the rotational symmetry. Whilst the exciton wavefunctions are very difficult to calculate precisely, we can use symmetry arguments to determine the number of distinct energy levels and their degeneracies for a single exciton complex, as well as the selection rules for transitions between energy levels belonging to two different exciton complexes. For this, we use group theory, which proved to be very useful in quantum mechanics and other branches of physics in the twentieth century thanks to the work of physicists such as Eugene Wigner and Hermann Weyl [12]. In our problem, we describe the symmetry of a QD by its *group of the Hamiltonian*, which is constructed from the set of all rotations and roto-inversions which commute with the Hamiltonian that governs exciton complexes.

In 2015, Karlsson *et al.* published a paper claiming that InGaAs QDs grown in a way which suggests their group of the Hamiltonian should be C_{3v} exhibit, for certain exciton transitions, spectral features which imply the group of the Hamiltonian to contain more symmetries, corresponding to D_{3h} or C_{6v} [10]. The effect of *symmetry elevation* has been studied by Karlsson *et al.* in [10] and [13] and by Dupertuis *et al.* in [14], but remains yet unexplained. In this work, we collaborate with a laboratory at Tyndall Institute, University College Cork, which reproduces the spectral measurements for this type of QDs using new methods of spectral feature identification. We compare these measurements to our simple perturbative model of *symmetry suppression* which attempts to quantify the effects of approximate symmetries, which were hypothesised by Dupertuis *et al.* as the mechanism behind symmetry elevation [14, p. 2]. Finally, we reject the suggested groups D_{3h} and C_{6v} as candidates for symmetry
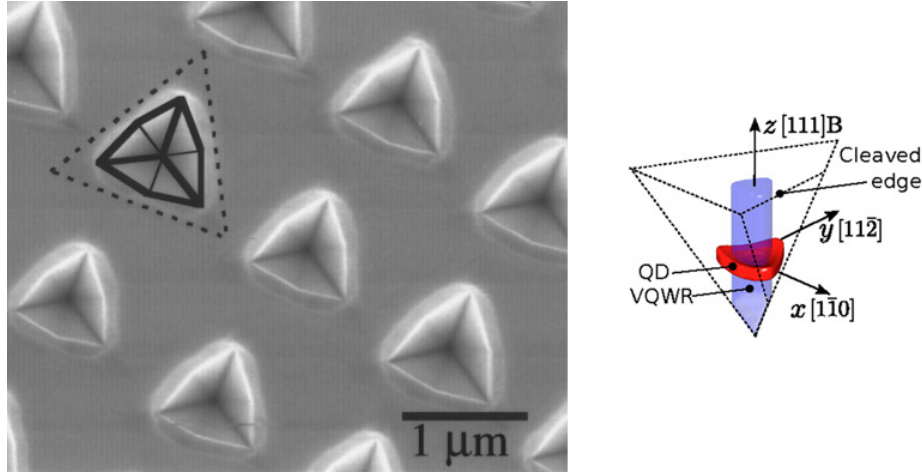
Figure 1: The tetrahedral recesses within which the QDs are grown. Dashed lines indicate the pyramid boundaries before growth, the solid lines indicate the vicinal facets after growth. "VQWR" refers to the vertical quantum wire present in the structure. Recess figure taken from [15, Fig. 1]; QD structure diagram taken from [10, Fig. 1]

elevation due to them postulating symmetries which the underlying atomic lattice of the QD is not equipped with. Instead, we identify T_d as the *bulk symmetry* of this lattice, and propose it as a new candidate for symmetry elevation. Bulk symmetry is the group of rotations and roto-inversions an exciton living in the crystal would possess if the crystal was of infinite volume.

3.1   The InGaAs pyramidal quantum dot

The quantum dot bulk is an $In_{0.10}Ga_{0.90}As$ alloy semiconductor, and the dot is grown in tetrahedral recesses on a GaAs $\{111\}B$ substrate. Within each tetrahedral recess, three quantum wires form along the pyramid corners, and a quantum dot forms at the tip of the pyramid where the quantum wires meet [15]. As seen in Fig. 1, the shape of the recess should determine the symmetries of the dot. The triangular base yields the three-fold rotation about the z-axis, and the inclination of the facets breaks the z-mirror symmetry. However, as seen by the deformation of the facets, the true shape of the dot is affected by several phenomena, some of which are poorly understood.

For instance, Holsgrove *et al.* [16] have studied a similar quantum dot which significantly differs only in the thickness of the lateral quantum wires, and have found the dot to form the shape of a regular hexagon, which does possess C_{6v} symmetry (see Fig. 2). We do not believe that our dot also forms a regular hexagon, and even in such case the true symmetry would be limited by the underlying lattice, hence disconfirming C_{6v} as the group towards which symmetry elevates. However, this illustrates that the true shape of the QD is poorly understood, and might exhibit properties which allow approximate symmetries to manifest.

Dupertuis *et al.* claim that symmetry elevation manifests in strain-free QDs [14,
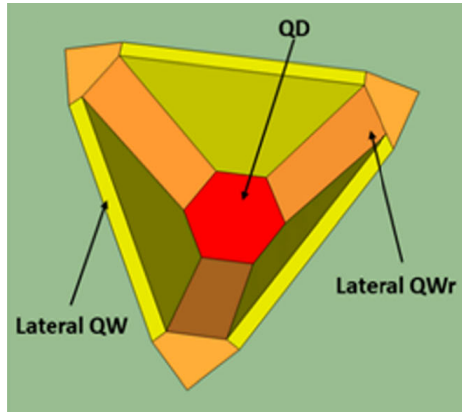
Figure 2: Analogously-grown QDs form regular hexagons. "QW" labels quantum wells, "QWr" labels quantum wires. Figure taken from [16, Fig. 1]

p. 4], and hence we disregard strain effects and symmetry breaking possibly caused by them in our analysis, and we discuss the possible effects of strain on our models in Sec. 6.4 and Sec. 7.

The measurements were conducted by our colleagues Francesco Mattana, Luca Colavecchi, Gediminas Juska and Emanuele Pelucchi (Tyndall National Institute, University College Cork). The data will be published together with the experimental details and descriptions of the methods they used to identify emission lines with the exciton transitions they correspond to in a separate paper, and therefore we omit this information here. Mattana, Colavecchi, Juska, and Pelucchi have kindly provided us with the results of their measurements of the spectral features of individual exciton decays, which we use to test our theoretical model in Sec. 5.4.2.

4 Discussions of theory employed

4.1 Exciton complexes and double groups

The physical phenomenon which is subject to our study is photoluminiscence. The QDs in a laboratory ensemble are arranged with large spacing and are not expect to interact, hence we can formulate a theoretical model of photoluminiscence on a singular QD. For InGaAs there are two valence bands at the band edge, which are close at Γ (see Fig. 3). These two valence bands have different curvatures at Γ, and hence correspond to holes of two different effective masses, referred to as heavy holes and light holes.

An external electromagnetic field in the form of a light-beam interacts with the QD in a non-resonant way (as for not to favour a single transition), which promotes electrons into the conduction band and holes into the valence bands. The population of excited electrons and holes of different characteristics is called an exciton complex. Exciton complexes decay into lower-occupancy exciton complexes via electron-hole recombination, which produces bright emission lines in the photoluminiscence spectrum. These lines are sharp and occur at fixed frequencies corresponding to the energy level difference between the initial and final state, and the theoretical description of their spectrum is the ultimate goal of this work.

Exciton complexes are labelled by the number of electron-hole pairs, overall charge, and the occupancy numbers of each hole type. For example, $2X_{20}^{-}$ has 3 electrons, 2 heavy holes, 0 light holes, and an overall charge of $-1e$.

The excitons with emissions resolvable in the analysed datasets have low occupancy numbers (3 or fewer of any of the three fermions–electrons, light holes, and heavy holes). Because InGaAs has a direct band-gap at Γ, we approximate the exciton complexes as living on the Γ point, i.e. each excited fermion having zero crystal momentum $\vec{k}$ (Fig. 3). Crystal momentum arises naturally in periodic lattices, since by Bloch's theorem the energy eigenfunctions in a periodic lattice have the form of a function periodic in the lattice modulated by a plane wave of which the associated wavevector $\vec{k}$ is called the crystal momentum vector [18, Ch. 2.2].

4.1.1 Envelope function method

The following approach is informed by that developed by Burt (1999), [19]. Let us consider a QD with a single excited electron which is promoted to the conduction band (the following easily generalises to holes promoted to valence bands). Disregarding the spin component of its wavefunction for simplicity, we decompose the electron's spatial wavefunction $\Psi\left(\vec{r}\right)$ into plane-waves:

$$\Psi\left(\vec{r}\right) = \int \mathrm{d}\vec{k}\,\tilde{\Psi}\left(\vec{k}\right) \exp\left\{i\vec{k}\cdot\vec{r}\right\} \tag{4.1}$$

where $\tilde{\Psi}\left(\vec{k}\right)$ is the Fourier transform of $\Psi\left(\vec{r}\right)$. From the crystal lattice we construct its reciprocal lattice, the set of vectors G such that a plane wave with a wavevector belonging to G is periodic in the crystal lattice [18, Ch. 2.6]. The first Brillouin
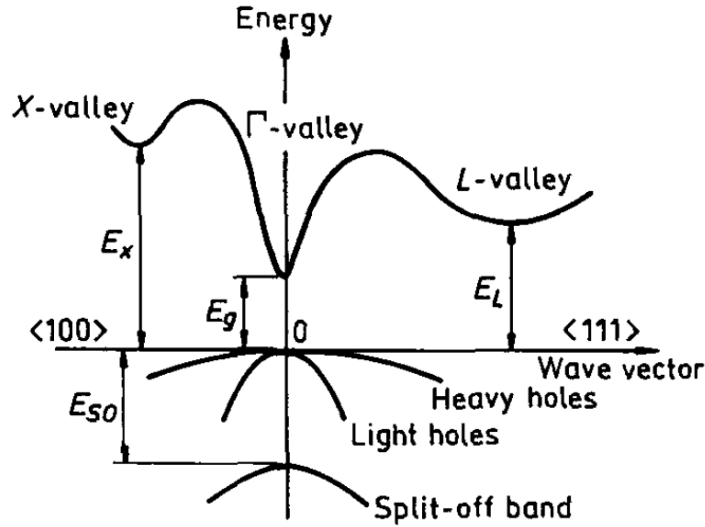
Figure 3: Band structure of the conduction and valence bands of $In_{1-x}Ga_xAs$. In a nanocrystal, the breaking of rotational symmetries may cause the heavy hole and light hole bands to split at Γ, being no longer degenerate there, as shown in Sec. 4.2.3. Figure taken from [17, Fig. 3.2.1]

zone (B.Z.) is then the unit cell of the reciprocal lattice at the origin, and we now decompose the integral domain into the first Brillouin zone summed over the set of reciprocal lattice vectors G:

$$\Psi\left(\vec{r}\right) = \sum_{\vec{g}\in G} \int_{\vec{k}\in 1\text{st B.Z.}} d\vec{k}\,\tilde{\Psi}\left(\vec{k}+\vec{g}\right) \exp\left\{i\left(\vec{k}+\vec{g}\right)\cdot\vec{r}\right\} \tag{4.2}$$

Note that G is equivalent to the set of wave-vectors of plane waves periodic on the crystal lattice. Therefore, we can choose a set of basis functions $U_n\left(\vec{r}\right)$ periodic on the crystal lattice like so:

$$U_n\left(\vec{r}\right) = \sum_{\vec{g}\in G} u_n\left(\vec{g}\right)\exp\{i\vec{g}\cdot\vec{r}\} \tag{4.3}$$

$$U_n\left(\vec{r}+\vec{r}_B\right) = \sum_{\vec{g}\in G} u_n\left(\vec{g}\right)\exp\{i\vec{g}\cdot\vec{r}\}\exp\{i\vec{g}\cdot\vec{r}_B\} = U_n\left(\vec{r}\right) \tag{4.4}$$

where $\vec{r}_B \in R$ is a lattice vector and $u_n\left(\vec{g}\right)$ are the coefficients of the decomposition of U_n into reciprocal lattice plane waves, chosen such that U_n are orthonormal. Then, inverting this decomposition, we obtain

$$\exp\{i\vec{g}\cdot r\} = \sum_n u_n\left(\vec{g}\right)^* U_n\left(\vec{r}\right) \tag{4.5}$$

which allows us to decompose the original wavefunction into a sum of the orthonormal basis vectors U_n and their envelope functions Υ_n:

$$\Psi\left(\vec{r}\right) = \sum_n \Upsilon_n\left(\vec{r}\right) U_n\left(\vec{r}\right) \tag{4.6}$$

$$\Upsilon_n\left(\vec{r}\right) = \sum_{\vec{g}\in G}\int_{\vec{k}\in\text{B.Z.}} \mathrm{d}\vec{k}\, u_n\left(\vec{g}\right)^* \tilde{\Psi}\left(\vec{k}+\vec{g}\right)\exp\left\{i\vec{k}\cdot\vec{r}\right\} \tag{4.7}$$

Now we choose $U_n\left(\vec{r}\right)$ to represent the band-edge eigenstates in the bulk structure. Using a tight-binding model with spin-orbit coupling, these wavestates can be labelled by three quantum numbers: total angular momentum j, its projection onto the z-axis j_z, and the orbital energy excitation ε_n, which we assume to be in the ground state in our system due to energy occupancy statistics (as we expect the population of states other than in the ground state to be negligible for a low-power light-source). Furthermore, the quantum number j is determined by the orbital angular momentum l, which is given by the electron configuration in each specific band, and the spin $s = 1/2$ determined for electrons and electron holes by their fundamental properties.

Photonic nanostructures can, on a small scale, cease to posses a standard band-structure, instead featuring e.g. flat bands. Dresselhaus *et al.* (2007) quotes the number of crystal lattice cells below which this occurs to be in the order of 10^2 [20, p. 213]. Our QDs have volumes typically higher than $100\,\text{nm}^3$ [13, p. 2], which corresponds to the number of unit cells in the order of 10^3. Hence we can reasonably expect our system to posses a band structure resembling the standard bulk-lattice band structure in the vicinity of Γ. This has two consequences to our envelope function model:

1. The envelope function $\Upsilon\left(\vec{r}\right)$ is varying slowly enough for it to have an approximately defined crystal momentum. As discussed in 4.1, we assume $k\approx 0$.

2. The wavefunction $\Psi\left(\vec{r}\right)$ of a single excited fermion approximately corresponds to a single state on the excited band of the band structure of the infinite bulk crystal lattice. In other words, there exists a basis vector U_n such that for all other basis vectors $U_m, m\neq n$, their contribution to the wavefunction is negligible. This postulate is equivalent to disregarding band-mixing effects.

Labelling the single contributing basis vector by the quantum numbers l, s, j, j_z, we can express the wavefunction of a single excited fermion as

$$\langle\vec{r}|\Psi\rangle = \Upsilon\left(\vec{r}\right)\langle\vec{r}|l, s = 1/2, j, j_z\rangle \tag{4.8}$$

4.1.2 Envelope-effective Hamiltonian at Γ

As discussed by Burt (1992) [21, p. 6656], we can write down the effective Hamiltonian for the envelope function, which yields the corresponding Schrödinger equation:

$$\hat{H}_\Upsilon = -\frac{\hbar^2}{2}\nabla\cdot\frac{1}{m^*\left(\vec{r}\right)}\nabla + E_0 \tag{4.9}$$

$$\hat{H}_\Upsilon\Upsilon\left(\vec{r}\right) = E\Upsilon\left(\vec{r}\right) \tag{4.10}$$

where E_0 is the band-edge energy. Now, in a parabolic Taylor expansion of the bands about Γ, we state that around the Γ point the effective mass m^* is constant. We now

see that the Schrödinger equation reduces to the following form:

$$-\frac{\hbar^2}{2m^*}\nabla^2\Upsilon = (E - E_0)\Upsilon \tag{4.11}$$

This is the equation of a free particle with energy $E_p = E - E_0$. Hence we can model a single excited fermion as a "particle in a box" around the Γ point for a large enough structure.

Now we consider the wavefunction of an exciton complex, which is comprised of multiple excited fermions. The interaction between the fermions is purely electromagnetic (disregarding the Pauli exclusion principle, which is treated in Sec. 4.2.4). Since the envelope functions are slowly-varying and associated to zero crystal momentum, their magnetic interaction is negligible. The magnetic interaction of the periodic basis functions gives rise to spin-orbit and orbit-orbit coupling (ignoring the hyperfine structure of spin-spin coupling), which allows us to label an exciton complex with a total angular momentum J and its projection onto the z-axis J_z as two quantum numbers. The Coulomb interaction between fermions a and b gives rise to a term in the Hamiltonian in the form

$$\hat{V}_{ab}^C (\vec{r}_a, \vec{r}_b) = \frac{q_a q_b}{4\pi\epsilon_0\epsilon_r} \frac{1}{|\vec{r}_a - \vec{r}_b|} \tag{4.12}$$

This operator can be rewritten as a function of a single vector:

$$\hat{V}_{ab}^C \left(\vec{\xi}\right) = \frac{q_a q_b}{4\pi\epsilon_0\epsilon_r} \frac{1}{\xi}, \qquad \xi = \left|\vec{\xi}\right| \tag{4.13}$$

Note that when this operator acts on the full two-particle wavefunction:

$$\hat{V}_{ab}^C (\vec{r}_a - \vec{r}_b)\, \Upsilon_a (\vec{r}_a)\, U_a (\vec{r}_a)\, \Upsilon_b (\vec{r}_b)\, U_b (\vec{r}_b) \tag{4.14}$$

the envelope functions Υ_a, Υ_b are slowly-varying, so we can state that they don't change in the volume of a single crystal lattice cell. Therefore, we can take the envelope functions outside of an integral over a domain where each vector $\vec{r}_a, \vec{r}_b$ is confined to a single cell:

$$\int_{\vec{r}_a \in \text{cell a}} \mathrm{d}^3\vec{r}_a \int_{\vec{r}_b \in \text{cell b}} \mathrm{d}^3\vec{r}_b \hat{V}_{ab}^C (\vec{r}_a - \vec{r}_b)\, \Upsilon_a (\vec{r}_a)\, U_a (\vec{r}_a)\, \Upsilon_b (\vec{r}_b)\, U_b (\vec{r}_b) \approx$$
$$\Upsilon_a (\vec{r}_a)\, \Upsilon_b (\vec{r}_b) \int_{\vec{r}_a \in \text{cell a}} \mathrm{d}^3\vec{r}_a \int_{\vec{r}_b \in \text{cell b}} \mathrm{d}^3\vec{r}_b \hat{V}_{ab}^C (\vec{r}_a - \vec{r}_b)\, U_a (\vec{r}_a)\, U_b (\vec{r}_b)$$

and since U_a, U_b are periodic over the crystal lattice, we can denote $\vec{\xi} = \vec{R}_{\text{cell b}} - \vec{R}_{\text{cell a}}$ to be the lattice vector equal to the displacement between the two cells, then the integral becomes

$$\int_{\vec{r}_a \in \text{cell a}} \mathrm{d}^3\vec{r}_a \int_{\vec{r}_b \in \text{cell b}} \mathrm{d}^3\vec{r}_b \hat{V}_{ab}^C (\vec{r}_a - \vec{r}_b)\, \Upsilon_a (\vec{r}_a)\, U_a (\vec{r}_a)\, \Upsilon_b (\vec{r}_b)\, U_b (\vec{r}_b) \approx$$
$$\Upsilon_a (\vec{r}_a)\, \Upsilon_b (\vec{r}_b) \int_{\vec{r}_a \in \text{U.C.}} \mathrm{d}^3\vec{r}_a \int_{\vec{r}_b \in \text{U.C.}} \mathrm{d}^3\vec{r}_b \hat{V}_{ab}^C \left(\vec{r}_a - \vec{r}_b - \vec{\xi}\right) U_a (\vec{r}_a)\, U_b (\vec{r}_b)$$

where U.C. denotes a single unit cell of the crystal lattice centered around the origin (or otherwise fixed in space). Now comes the final approximation. When considering the integral of Eq. (4.14) over an arbitrary dual volume, we partition the volumes into unit cells of the crystal lattice and then divide the integral into pairwise U.C.-U.C. integrals over a set of displacement vectors $\vec{\xi}$. For the majority of these vectors in dual volumes comparable in size to the size of the QD, the values of ξ will be larger than the dimensions of the U.C. Hence we can approximate

$$\hat{V}_{ab}^C\left(\vec{r}_a - \vec{r}_b - \vec{\xi}\right) \approx \hat{V}_{ab}^C\left(\vec{\xi}\right) \tag{4.15}$$

By denoting the set of lattice vectors in the volume V as R_V, the integral simplifies to

$$\int_V \mathrm{d}^3\vec{r}_a \int_V \mathrm{d}^3\vec{r}_b \hat{V}_{ab}^C\left(\vec{r}_a - \vec{r}_b\right) \Upsilon_a\left(\vec{r}_a\right) U_a\left(\vec{r}_a\right) \Upsilon_b\left(\vec{r}_b\right) U_b\left(\vec{r}_b\right) \approx$$
$$\Pi_{ab} \sum_{\vec{r}_a \in R_V} \sum_{\vec{r}_b \in R_V} \hat{V}_{ab}^C\left(\vec{r}_a - \vec{r}_b\right) \Upsilon_a\left(\vec{r}_a\right) \Upsilon_b\left(\vec{r}_b\right)$$

where $\quad \Pi_{ab} = \int_{\vec{r}_a \in \text{U.C.}} \mathrm{d}^3\vec{r}_a \int_{\vec{r}_b \in \text{U.C.}} \mathrm{d}^3\vec{r}_b U_a\left(\vec{r}_a\right) U_b\left(\vec{r}_b\right) \quad$ is a correlation constant.

Now we renormalize the correlation constant Π_{ab} using the volume of the unit cell $V_{\text{U.C.}}$, which allows us to rewrite the double sum over R_V as an integral over the dual volume:

$$\int_V \mathrm{d}^3\vec{r}_a \int_V \mathrm{d}^3\vec{r}_b \hat{V}_{ab}^C\left(\vec{r}_a - \vec{r}_b\right) \Upsilon_a\left(\vec{r}_a\right) U_a\left(\vec{r}_a\right) \Upsilon_b\left(\vec{r}_b\right) U_b\left(\vec{r}_b\right) \approx$$
$$\Pi_{ab}' \int_V \mathrm{d}^3\vec{r}_a \int_V \mathrm{d}^3\vec{r}_b \hat{V}_{ab}^C\left(\vec{r}_a - \vec{r}_b\right) \Upsilon_a\left(\vec{r}_a\right) \Upsilon_b\left(\vec{r}_b\right),$$
$$\text{where} \quad \Pi_{ab}' = V_{\text{U.C.}}^{-2} \Pi_{ab} = \langle U_a\left(\vec{r}_a\right) U_b\left(\vec{r}_b\right)\rangle_{\text{U.C.}}$$

Since this must be true for any (sufficiently large) V, we drop the integral altogether, equating the integrands:

$$\hat{V}_{ab}^C\left(\vec{r}_a - \vec{r}_b\right) \Psi_a\left(\vec{r}_a\right) \Psi_b\left(\vec{r}_b\right) = \Pi_{ab}' \hat{V}_{ab}^C\left(\vec{r}_a - \vec{r}_b\right) \Upsilon_a\left(\vec{r}_a\right) \Upsilon_b\left(\vec{r}_b\right) \quad \text{on vol. avg.} \tag{4.16}$$

What was done here was essentialy taking a volume average over the product of the basis functions $U_a U_b$, motivated by their periodicity over unit volumes much smaller than that of the quantum dot. This high-frequency periodicity manifests as a simple correlation coefficient when considering matrix elements of $\hat{V}_{ab}^C$.

   This allows us to modify Eq. (4.11) to account for Coulomb interaction purely in the paradigm of envelope functions. The full effective Schrödinger equation for envelope functions (since the fine structure effects do not matter for the slowly-varying envelope functions) is then

$$\left(-\sum_i \frac{\hbar^2}{2m_i^*} \nabla_{\vec{r}_i}^2 + \sum_{i,j;i\neq j} \Pi_{ij}' \hat{V}_{ij}^C\left(\vec{r}_i - \vec{r}_j\right)\right) \Upsilon = E_{\text{exciton}} \Upsilon \tag{4.17}$$

where

$$\Upsilon = \prod_i \Upsilon_i\left(\vec{r}_i\right)$$

Note that the Coulomb interaction on the volumes of the scale of the unit cell of the crystal lattice is fully rotationally symmetric, and therefore will not invalidate J, J_z as good quantum numbers. However, it will affect the value of Π'_{ij}, which therefore becomes nontrivial to calculate. It will also affect the shape of the periodic functions, which we can for simplicity just denote $F_i\left(\vec{r}_i\right)$, and which have the same periodic properties as $U_i\left(\vec{r}_i\right)$, and form in totality a J, J_z eigenstate. Therefore, we expect the transformation $U_i \to F_i$ to only affect the radial dependence in the close vicinity of an atom, preserving the spherical-harmonics angular dependence in the tight-binding model.

By interpreting Eq. (4.17), we now see that the envelope functions in an exciton complex behave as free particles in a box with added Coulomb interactions, i.e. a many-body charged particle system. Note that the potential barriers at the edges of the "box" are not infinite, and that would indeed not be a good approximation!

Note. Even though $\hat{V}^C_{ab}\left(\vec{r}_a - \vec{r}_b\right)$ diverges for $\vec{r}_a = \vec{r}_b$ (which occurs in the small subset of $R_V \otimes R_V$ where both vectors are in the same unit cell), the contribution of the integrals over these coinciding unit cells should not be disproportionally high, since when considering the volume integral in spherical coordinates centered on the asymptote, the integrand goes like $|\vec{r}_a - \vec{r}_b|$, so the integral should be approximately proportional to $V^{2/3}_{\text{U.C.}}$, and the contribution from this subset where our approximations fail to the total integral is negligible.

4.2 Symmetry in quantum dots

Now that we have decomposed the single excited fermion wavefunction into a j-eigenstate periodic in the atomic lattice and a slowly varying envelope function which corresponds to zero bulk-crystal momentum, we turn to symmetry arguments to make predictions about the spectrum. Indeed, finding either of the two component functions is a task beyond the scope of this work, but we can make quantitative statements about the splitting of the exciton energy levels and selection rules for transitions between these energy levels. To do this, we must consider how the exciton wavefunction transforms under symmetry transformations of the true Hamiltonian.

4.2.1 Group theory–the formalism of symmetries

A *group* is a set of objects G equipped with a binary operation (here denoted $\cdot$ and referred to as *multiplication*) which satisfies the following requirements [22, Ch. 1]:

1. *Closure*: If g_1, g_2 are elements of G, then $g_1 \cdot g_2$ is an element of G.

2. *Associativity*: The order in which one evaluates multiplication of multiple elements does not matter; $(g_1 \cdot g_2) \cdot g_3 = g_1 \cdot (g_2 \cdot g_3)$.

3. *Identity*: There exists a neutral element $e \in G$ such that $e \cdot g = g$ for all $g \in G$.

4. *Inverse*: Each $g \in G$ has its inverse $g^{-1} \in G$ such that $g \cdot g^{-1} = e$.

A *representation* Γ (rep) is a mapping of group elements g onto matrices $D^{(\Gamma)}(g)$ of dimension $\dim \Gamma$ that preserves the group operation as matrix multiplication [22, Ch. 2]:

$$D^{(\Gamma)}(g_1)D^{(\Gamma)}(g_2) = D^{(\Gamma)}(g_1 \cdot g_2) \tag{4.18}$$

The *character* of element g in representation Γ is the trace of its matrix:

$$\chi^{(\Gamma)}(g) = \mathrm{Tr}\, D^{(\Gamma)}(g) \tag{4.19}$$

A representation is *reducible* if there exist a similarity transformation which simultaneously brings the matrix of every element into block-diagonal form:

$$D(g) \to P^{-1}D(g)P = \begin{pmatrix} D_1(g) & 0 \\ 0 & D_2(g) \end{pmatrix} \tag{4.20}$$

When multiplying two block-diagonal matrices of equal structure, the elements from different blocks are decoupled, and hence $D_1(g)$ and $D_2(g)$ form two new, lower-dimensional representations of G. A representation which cannot be reduced in this way is called *irreducible* (irrep). There is a finite number of irreps for a finite group, and the tables of their characters for each element for point groups (groups formed on rotations of geometric structures) are included in [23].

In a vector space where each dimension corresponds to one group element, the characters of an irrep form a vector. These vectors are orthonormal with norm $|G|$ [22, Ch. 3]. This allows us to uniquely reduce any representation into its constituent irreps, as if decomposing a general vector into a basis.

A set of objects $|\Gamma, i\rangle$, $i = 1, 2, \ldots \dim \Gamma$ forms a basis to Γ if it transforms according to its matrices [22, Ch. 4]:

$$g \begin{pmatrix} |\Gamma, 1\rangle \\ |\Gamma, 2\rangle \\ \vdots \\ |\Gamma, \dim \Gamma\rangle \end{pmatrix} = D^{(\Gamma)}(g) \begin{pmatrix} |\Gamma, 1\rangle \\ |\Gamma, 2\rangle \\ \vdots \\ |\Gamma, \dim \Gamma\rangle \end{pmatrix} \tag{4.21}$$

To review the basic applications of group theory to quantum mechanics [22, Ch. 5]: the set of symmetry transformations $\hat{P}_R$ commuting with a Hamiltonian $\hat{H}$ forms a group under multiplication, denoted $G_{\hat{H}}$, which is referred to as the group of the Hamiltonian. Each energy level E_n of the time-independent Schrödinger eigenvalue problem $\hat{H}\Psi_n = E_n\Psi_n$ corresponds to an irreducible representation of $G_{\hat{H}}$, which we can denote as $\Gamma_{r(n)}$, where r is some mapping. A chosen basis of degenerate eigenstates $|E_n, i\rangle$ is also a basis of $\Gamma_{r(n)}$. The degeneracy of E_n is then equal to the dimension of $\Gamma_{r(n)}$. Therefore, knowing the group of the Hamiltonian tells us the possible degeneracies of the energy levels and what they transform as under the symmetry transformations.

Moreover, group theory has an application to selection rules. Consider two energy levels E_a, E_b of a system with the Hamiltonian $\hat{H}$. If we add a perturbation $\hat{H}'$ which allows transition between energy levels, and which transforms according to

the representation $\Gamma_{\hat{H}'}$, by Fermi's golden rule the rate of transition $E_a \to E_b$ is proportional to the matrix element $\langle E_a | \hat{H}' | E_b \rangle$ [24, Eq. (3.2)]. As per [22, Ch. 7], this matrix element vanishes if the irrep direct product $\Gamma_{r(a)} \otimes \Gamma_{\hat{H}'} \otimes \Gamma_{r(b)}$ does not contain the identity representation. This allows us to decide which exciton transitions under photoluminiscent electron-hole recombination will be dark in which polarisation.

4.2.2   Symmetries of quantum dots and double groups

Consider now the symmetries of the envelope function $\Upsilon = \prod_i \Upsilon_i(\vec{r}_i)$ and the periodic function $F = \prod_i F_i(\vec{r}_i)$, respectively.

1. Υ, representing a many-body charged particle-in-a-box system, is governed in its symmetry by the shape of the box, i.e. the shape of the QD. In our system, this shape is assumed to posses C_{3v} (pyramid with equilateral triangle base) symmetry. This symmetry shall be referred to as the *structure symmetry*.

2. F, representing a function periodic in the crystal lattice, is governed in its symmetry by the shape of the lattice, i.e. the properties of the bulk of the crystal. In our system, the crystal lattice is a zincblende structure (cubic FCC) [17, p. 62] oriented along the [111] direction. The point group of this lattice is T_d (regular tetrahedron) [25]. This symmetry shall be referred to as the *bulk symmetry*.

3. Around the individual atoms in the crystal lattice, in the tight-binding model the exciton forms a total angular momentum eigenstate $|J, J_z\rangle$. This has a full roto-inversion symmetry, and since it couples spin-half spinors, which transform according to the fundamental representation of $SU(2)$ under inversions [26, p. 228], the group describing the full roto-inversion symmetry is $SU(2) \otimes C_i$, where $C_i = \{\hat{E}, \hat{i}\}$ is the inversion group and it is isomorphic to $\mathbb{Z}_2$.

The group of the true Hamiltonian is then constructed from symmetry transformations present in all of these groups. Because the crystal lattice of the QD is oriented along the [111] direction, it contains every structure-symmetry transformation. Therefore the true symmetry is the structure symmetry C_{3v}–or rather, since we are considering spin-half spinors, its double group, as will be discussed below. However, as we argue below, the bulk symmetry will be important when explaining the origin of symmetry elevation in our perturbative model.

Now, let us consider the character of the full exciton wavefunction under a symmetry transformation $\hat{R}$. Since the Coulomb interaction transforms according to the identity rep under roto-inversions, we can first consider the character of a single fermion wavefunction under the symmetry transformation, and then we construct the full exciton character through j-coupling, as discussed in Sec. 4.2.3. Since the single excited fermion wavefunction is a product of two functions, its character will be the product of the two constituent characters:

$$\chi^{(\Psi(\vec{r}))}\left(\hat{R}\right) = \chi^{(\Upsilon(\vec{r}))}\left(\hat{R}\right) \chi^{(U(\vec{r}))}\left(\hat{R}\right) \tag{4.22}$$
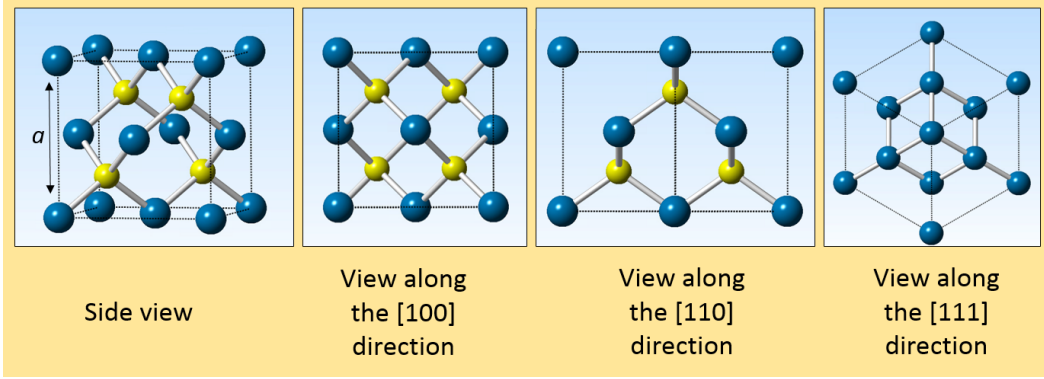
Figure 4: Zincblende lattice structure. Atoms of equal type are second-nearest neighbours, and thus a rotation which maps equal-type atoms onto themselves keeps the lattice-periodic component of the exciton wavefunction constant. Figure taken from [28, Fig. 2.3]

The character of the envelope function can be, in principle, any irrep of the structure symmetry group. However, we once again invoke the energy statistics–the population of QDs excited by a low-energy laser for which the envelope functions are out of the ground state should be negligible. Therefore, assuming the envelope function is in its ground state, we know it transforms according to the identity rep. Therefore $\chi^{(\Upsilon(\vec{r}))}\left(\hat{R}\right) = 1$.

In the tight-binding model, the band-edge eigenstate U is a convolution of the j-eigenstate which exists around each atom with the distribution of the atoms, weighted relatively to their atomic properties. Since the structure symmetry group is a subgroup of the bulk symmetry group, the bulk crystal lattice maps onto itself under every rotation in the structure symmetry. Furthermore, the Ga-As bonds in the conduction band are antisymmetric, and the second-nearest neighbour bonds are symmetric [27], which leaves the lattice to transform according to the identity rep (Fig. 4).

Therefore the only part of the single excited fermion wavefunction which does not necessarily transform according to the identity rep is the j-eigenstate itself. The character of a j-eigenstate under any rotation is the trace of the corresponding Wigner D-matrix, the general irrep $\Gamma_j^{(SU(2))}$ of $SU(2)$ derived by Wigner in [26, Ch. 15] and each set of eigenstates

$$\begin{pmatrix} |j, j_z = j\rangle \\ |j, j_z = j - 1\rangle \\ \vdots \\ |j, j_z = -j\rangle \end{pmatrix} \text{ forms a basis to } \Gamma_j^{(SU(2))}$$

To extend this unto roto-inversions, we need to consider the orbital angular momentum l, which determines inversion parity. For example, in our system, the conduction band is an s-orbital, which has even parity under inversion, but the valence band is a p-orbital, which has odd parity under inversion. Determining parity specifies the

irrep of the full roto-inversion group $SU(2) \otimes C_i$, which gains an index g (gerade) if even or u (ungerade) if odd under inversion.

Our approach to constructing the transformation laws for the single excited fermions is therefore to consider the irreps of the full roto-inversion spinor group, and then decompose them into the true symmetry, i.e. the structure symmetry. To do this, we must construct the double group of the structure symmetry point group. Essentially, a double group includes the transformation properties of half-integer j eigenstates, and thus allowing the description of spin-orbit coupling for its original group by adding the time-reversal operator as a generator. Then, rotations by 2π result in time-reversal, adding a factor of -1 to half-integer j-eigenstates, and only rotations by 4π return back to the identity, in agreement with the behaviour of spin-half particles under rotation. The theory of double groups is outlined in [22, Ch. 19], and the character tables of double groups can be found in standard tables, such as [23].

4.2.3 Total angular momentum coupling

To obtain the transformation properties of an exciton complex, we must consider the magnetic orbit-orbit and spin-orbit interaction which couples the total angular momenta j of separate fermions together (Sec. 4.1.2). The treatment of j-coupling in the full roto-inversion symmetry is as follows:

Consider two non-interacting particles governed by Hamiltonians which conserve total angular momentum. Let the two particles exist in j-eigenstates $\left|j^A, j_z^A, p^A\right\rangle$, $\left|j^B, j_z^B, p^B\right\rangle$ respectively (here p specifies the inversion parity), and the group of each of their Hamiltonians is $SU(2) \otimes C_i$. The full Hilbert space they occupy is the direct product of the Hilbert space occupied by each particle, and hence the group of the total Hamiltonian is:

$$G_{\hat{H}}^{\text{non-int.}} = (SU(2) \otimes C_i) \otimes (SU(2) \otimes C_i) \tag{4.23}$$

The irreps of this group are the direct products of the respective irreps $\Gamma_{j,p}$, and hence

$$\left|j^A, j_z^A, p^A\right\rangle \otimes \left|j^B, j_z^B, p^B\right\rangle \quad \text{transforms according to} \quad \Gamma_{j^A, p^A} \otimes \Gamma_{j^B, p^B} \tag{4.24}$$

If we now include an interaction term in the full Hamiltonian which couples the total angular momenta of the particles, j_z^A, j_z^B cease to be good quantum numbers. Instead (in classic electromagnetic coupling), the full total angular momentum J and its projection along the z-axis, J_z, become good quantum numbers. Preserving j^A, j^B as immutable parameters of the physical system, the new energy eigenstates posses the roto-inversion symmetry $SU(2) \otimes C_i$, and transform according to its irreps. Hence we need to reduce the high-symmetry irrep in Eq. (4.24) into the lower-symmetry group $SU(2) \otimes C_i$.

We will assume that all constituent irreps in the decomposition have equal parity, which is the product of the two parities $p^A \cdot p^B$. Then, using standard results [26,

Ch. 17], we write down the decomposition:

$$\Gamma_{j^A,p^A} \otimes \Gamma_{j^B,p^B} = \sum_{J=|j^A-j^B|}^{j^A+j^B} \Gamma_{J,p^A \cdot p^B} \tag{4.25}$$

The fact that this equation holds justifies our assumption about coupling inversion parity, since a decomposition is unique.

Using this equation, we see that excited electrons, which couple their intrinsic $s = 1/2$ angular momentum to the $l = 0$ angular momentum of the conduction band s-orbital transform like $\Gamma_{j=1/2,g}$. Similarly, excited holes coupling their $s = 1/2$ angular momentum to the $l = 1$ angular momentum of the valence band p-orbital transform like $\Gamma_{j=1/2,u} \oplus \Gamma_{j=3/2,u}$. The heavy-hole band, the light-hole band, and the split-off band transform as $|3/2, \pm 3/2\rangle$, $|3/2, \pm 1/2\rangle$, $|1/2, \pm 3/2\rangle$, respectively [18, Eq. (2.54-56)]. Identifying $\Gamma_{j=1/2,u}$ as the irrep of the split-off band, which has too small energy to have a hole promote to it instead of to a heavy or light hole band (Fig. 3), we are left with $\Gamma_{j=3/2,u}$ for the heavy and light holes.

Reducing these representations into the C_{3v} double group, we obtain the irrep $E_{1/2}$ for electrons and the rep $E_{1/2} \oplus E_{3/2}$ for heavy and light holes. Considering how each pair of basis vectors $|3/2, \pm 3/2\rangle$, $|3/2, \pm 1/2\rangle$ transforms under rotations, e.g. by comparing the subtraces of $\Gamma_{j=3/2,u}$ at indices $i = 1,4$ and $i = 2,3$, respectively, to the traces of $E_{1/2}$ and $E_{3/2}$, we identify $E_{3/2}$ as the irrep of the heavy-hole band and $E_{1/2}$ as the irrep of the light-hole band. This illustrates that in a nanocrystal with C_{3v} symmetry, the heavy hole and light hole bands undergo splitting, no longer being degenerate at Γ.

We can now generalise the approach to j-coupling to cases where each particle's original Hamiltonian undergoes symmetry breaking to some double group $\tilde{G}_{\hat{H}_0}$, which is a subgroup of $SU(2) \otimes C_i$. In the non-interacting direct product of the two Hilbert spaces, each pair of quantum numbers j^i, j_z^i reduces into an instance of this subgroup, and so the pair of non-interacting particles transforms according to $\tilde{G}_{\hat{H}_0} \otimes \tilde{G}_{\hat{H}_0}$. If we include the j-coupling interaction term, the full system features only one pair of these quantum numbers, J, J_z, which reduce into a single instance of the aforementioned subgroup. Hence, the reduction goes like this:

$$\Gamma_A^{(\tilde{G}_{\hat{H}_0})} \otimes \Gamma_B^{(\tilde{G}_{\hat{H}_0})} \rightarrow \bigoplus_i \Gamma_{f(i)}^{(\tilde{G}_{\hat{H}_0})} \tag{4.26}$$

where the mapping $f(i)$ specifies the decomposition. Naturally, as the constituent irreps in the direct sum on the right side correspond to different energy levels (disregarding accidental degeneracy), the symmetry breaking associated with coupling of quantum numbers lowers the degeneracy of the system.

4.2.4 J-eigenstate transformations with the Pauli exclusion principle

The outlined method is sufficient for finding the energy levels of distinguishable particles undergoing coupling; however, in our case, the particles are fermions, and

hence, for particles occupying the same k-state in the same band, we also have to consider Pauli exclusion principle.

As discussed in Sec. 4.2.3, the electrons promoted to the conduction band have $j = 1/2$, which renders their k-states doubly degenerate, and the holes promoted to the heavy-hole and light-hole valence bands have $j = 3/2$ and a 4-fold degenerate k-state at Γ. However, for certain groups, including C_{3v}, the $SU(2) \otimes C_i$ irrep $\Gamma_{j=3/2,u}$ reduces to two 2-dimensional irreps, which causes light holes and heavy holes to occupy different energy levels at Γ, each with doubly degenerate k-states. We assume that the bands fill up sequentially under excitation in a way that maximises the number of completely filled-out states.

- For doubly degenerate k-states, we only need to find the transformation properties of the full k-state, i.e. a pair of fermions. As per Karlsson *et al.* [10, p. 15], a full doubly degenerate energy level transforms according to the identity representation.

- For 4-fold degenerate k-states with $j = 3/2$, we can extend Karlsson's argument to claim that the full energy level with 4 particles transforms according to the identity representation. We can label an energy level with 3 particles by the 1 missing particle, and hence it transforms equally to an energy level filled with 1 particle. Finally, for two particles, we need to construct the 6 antisymmetric basis vectors, with kets labelled by the j_z values of the first and the second particle respectively:

$$b_1 = \tfrac{1}{\sqrt{2}} \left(\left| \tfrac{3}{2}, -\tfrac{3}{2} \right\rangle - \left| -\tfrac{3}{2}, \tfrac{3}{2} \right\rangle \right) \quad b_2 = \tfrac{1}{\sqrt{2}} \left(\left| \tfrac{1}{2}, -\tfrac{1}{2} \right\rangle - \left| -\tfrac{1}{2}, \tfrac{1}{2} \right\rangle \right)$$
$$b_3 = \tfrac{1}{\sqrt{2}} \left(\left| \tfrac{3}{2}, \tfrac{1}{2} \right\rangle - \left| \tfrac{1}{2}, \tfrac{3}{2} \right\rangle \right) \qquad b_4 = \tfrac{1}{\sqrt{2}} \left(\left| -\tfrac{3}{2}, -\tfrac{1}{2} \right\rangle - \left| -\tfrac{1}{2}, -\tfrac{3}{2} \right\rangle \right)$$
$$b_5 = \tfrac{1}{\sqrt{2}} \left(\left| \tfrac{3}{2}, -\tfrac{1}{2} \right\rangle - \left| -\tfrac{1}{2}, \tfrac{3}{2} \right\rangle \right) \quad b_6 = \tfrac{1}{\sqrt{2}} \left(\left| -\tfrac{3}{2}, \tfrac{1}{2} \right\rangle - \left| \tfrac{1}{2}, -\tfrac{3}{2} \right\rangle \right)$$

The character of a rotation is given purely by the angle θ, not by the rotation axis, as

$$\chi^{(\Gamma_j)} \big(\hat{R}(\theta) \big) = \frac{\sin (2j + 1) \, \theta/2}{\sin \theta/2} \tag{4.27}$$

which is just the trace of the Wigner d-matrix, which Wigner defined as

$$d^{j}_{m',m} = \langle j, m' | \hat{R}(\theta) | j, m \rangle \tag{4.28}$$

where θ is the second Euler angle in the z-y-z convention [26, p. 160], and for which Wigner gave an expression [26, p. 167]. The character of a simultaneous rotation of two particles is a product of the two single-particle rotation characters, which allows us to calculate the sum of the simultaneous-rotation characters over all basis vectors:

$$\sum_{i=1}^{6} \chi^{b_i} \big(\hat{R}(\theta) \big) = 2 \cos \theta + 2 \cos 2\theta + 2 \tag{4.29}$$

which we can equate to the sum of the characters of $\Gamma_{j=0} \oplus \Gamma_{j=2}$, as per Eq. (4.27). Hence an energy level with $j = 3/2$ occupied by two particles transforms as $\Gamma_{j=0} \oplus \Gamma_{j=2}$.

Hence we can label any exciton complex for groups which have one or two hole characters by labelling each fermion type by the number of free fermions and then multiplying the corresponding representations for each fermion type. Reducing this into the irreps of the structure symmetry group gives the number of energy levels and their degeneracies for each exciton complex (Fig. 5).

4.3   Photoluminiscence spectrum and evidence of symmetry elevation

To predict the rate of photoluminiscent transitions between energy levels, we utilize the dipole approximation, in which the dipole operator (and hence the perturbing Hamiltonian) transforms as a vector [10, p. 13]. Vectors transform according to the Cartesian representation, which can be easily constructed from rotation matrices [26, p. 160]. If the Cartesian representation is reducible in the structure symmetry group, different vector orientations of the dipole may transform differently, resulting in different lines in polarised spectra. In that case, we must apply the selection rules outlined in Sec. 4.2.1 for each polarisation separately. Then, the number of allowed transitions between different finely-split energy levels of two excitons gives the number of tightly-spaced lines we predict on the spectrum of that exciton transition.

For the assumed symmetry C_{3v}, vectors $\hat{x}, \hat{y}$ transform differently to $\vec{z}$, meaning the spectrum polarised along the z-axis will be different than the spectrum polarised in the $x - y$ plane (σ-polarised). In the experiment, readings for both polarisations are collected, utilising a rotatable waveplate [10, p. 2].

In [10], Karlsson *et al.* have applied the selection rules to different exciton transitions and compared the predicted number of lines to their experimental data. The predictions have mostly agreed, but three exciton transitions were identified for which emission lines in the measured spectra were missing (Fig. 6). These were:

1. $X_{10} \rightarrow$ vacuum (2 predicted $x - y$-polarised lines, 1 measured).

2. $2X_{20} \rightarrow X_{10}$ (2 predicted $x - y$-polarised lines, 1 measured).

3. $2X_{11} \rightarrow X_{01}$ (6 predicted $x - y$-polarised lines, 3 resolved strongly and 2 more resolved weakly).

$$C_{3v} \quad 3X_{21} \xrightarrow{\text{Pauli exc.}} \begin{matrix} 1 \text{ free e.: } E_{1/2} \\ 0 \text{ free hh.: } A_1 \\ 1 \text{ free lh.: } E_{1/2} \end{matrix} \longrightarrow E_{1/2} \otimes E_{1/2} \xrightarrow{j\text{-coupling}} A_1 \oplus A_2 \oplus E$$

$$T_d \quad 2X_{11}^- \xrightarrow{\text{Pauli exc.}} \begin{matrix} 1 \text{ free e.: } E_{1/2} \\ 2 \text{ free h.: } A_1 \oplus E \oplus T_2 \end{matrix} \xrightarrow{j\text{-coupling}} E_{1/2} \oplus E_{5/2} \oplus F_{3/2} \oplus F_{3/2}$$

Figure 5: The process of labelling exciton complexes with irreps of the group of the Hamiltonian. T_d has both hole types degenerate at Γ, and thus they occupy a single quadruply-degenerate energy level (Tab. 2).

Karlsson *et al.* theorise that the missing lines or the relative intensity of lines in these transitions can be explained by a symmetry elevation to a larger group of symmetries of which C_{3v} is a subgroup. In our work, we have attempted to test this claim and identify the mechanism that employs the system with extra symmetries.
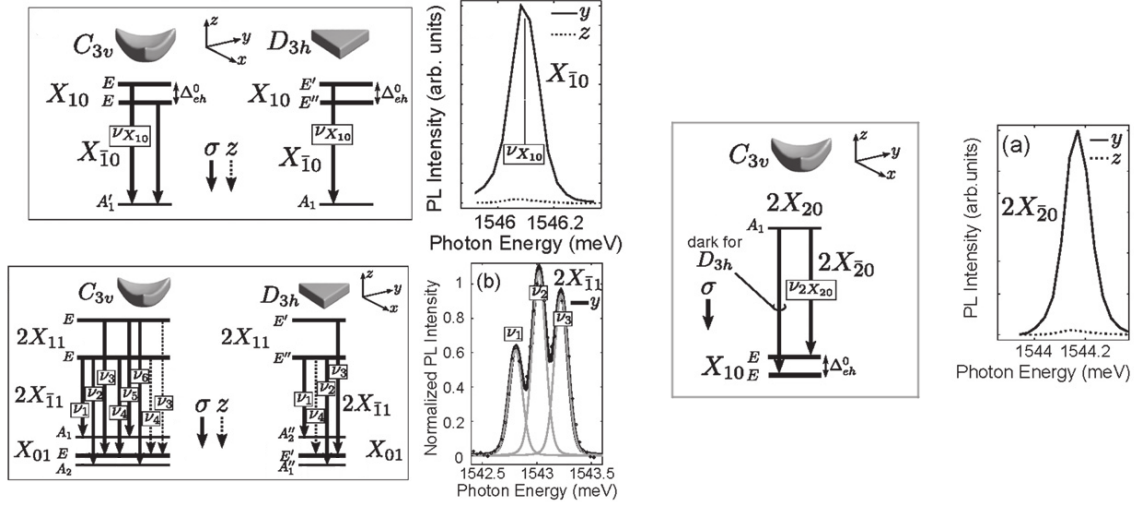

Figure 6: Evidence of symmetry elevation in the research of Karlsson *et al.*, with D_{3h} proposed as the elevated symmetry group. Energy level splitting and allowed transitions for three exciton complexes are plotted for the groups C_{3v} and D_{3h}, and identification of emission lines in the spectra is attempted. Figure taken from [10, Fig. 14, 15, 16]

5 Results

In our research, we tested the following hypothesis: *Symmetry elevation effects are caused by transformation properties of the bulk symmetry.* Since the bulk symmetry group T_d contains the structure symmetry C_{3v} as a subgroup, it is a natural suspect for a source of *approximate* symmetries, as it limits the true symmetry of the system.

The theoretical basis for particular excitons enjoying symmetry transformations from the bulk symmetry is built on their localisation within the QD. If the envelope functions Υ_i of every fermion in an exciton complex are localised near the centre of the QD, any bulk-symmetry transformation should also be a symmetry transformation of the exciton wavefunction. With every QD border the envelope functions approach, more approximate symmetry transformations vanish, until, when an exciton has significant probability to measure one or more of its fermions anywhere around the edge of the QD, it fully probes the structure symmetry.

5.1 Perturbative analysis of selection rules

Suppose now we have a system described by a Hamiltonian $\hat{H}$ equipped with a group of symmetries G. Let us construct a Hamiltonian $\hat{H}_+$ which is equipped with a group of symmetries G_+ such that $G \subset G_+$ and $\hat{H}$ can be modelled as a perturbation of $\hat{H}_+$ like so:

$$\hat{H} = \hat{H}_+ + \lambda\hat{H}', \quad \text{where} \quad \lambda \ll 1 \tag{5.1}$$

For an exciton with its wavefunction localised in the centre of the QD, $\hat{H}$ is the true Hamiltonian, and $\hat{H}_+$ is the Hamiltonian of a smaller QD with a higher symmetry inscribed into the true QD.

5.1.1 Elevated symmetry component of an energy eigenstate

Let us denote the eigenstates of the Hamiltonians $\hat{H}, \hat{H}_+$ as $|E_i; n\rangle$ and $\left|E_{i'}^+; n'\right\rangle$ respectively, where n, n' are the degeneracy labels. Disregarding accidental degeneracy, we know that every set of degenerate energy levels forms a basis of (i.e. transforms according to) an irrep of the respective symmetry group [22, Ch. 5]:

$$\begin{pmatrix} |E_i; 1\rangle \\ |E_i; 2\rangle \\ \vdots \\ |E_i; d_i\rangle \end{pmatrix} \text{ forms a basis to } \Gamma_{r(i)}^{(G)}; \quad \begin{pmatrix} \left|E_{i'}^+; 1\right\rangle \\ \left|E_{i'}^+; 2\right\rangle \\ \vdots \\ \left|E_{i'}^+; d_{i'}^+\right\rangle \end{pmatrix} \text{ forms a basis to } \Gamma_{r^+(i')}^{(G_+)} \tag{5.2}$$

where $d_i, d_{i'}^+$ specify the total degeneracies of the energy levels and r, r^+ are some functions which map energy levels onto irreps. Under a first-order perturbation of a set of degenerate eigenstates which span a Hilbert subspace $\mathcal{D}^+$, the distance of the perturbed states from $\mathcal{D}^+$ goes like $O(\lambda)$. Therefore, if $|E_i; n\rangle$ arises from perturbing a degenerate subspace of energy E_j^+, there exists an unnormalized vector

$\left|E_j^+; P\right\rangle \in \mathcal{D}_j^+$ for which

$$\frac{\left\langle E_i; n \middle| E_j^+; P\right\rangle}{\left|\left\langle E_j^+; P \middle| E_j^+; P\right\rangle\right|^{1/2}} = 1 - O(\lambda) \tag{5.3}$$

$$\text{where} \quad \left\langle E_j^+; P' \middle| E_i; n\right\rangle = \left\langle E_j^+; P' \middle| E_j^+; P\right\rangle \quad \text{for all} \quad \left|E_j^+; P'\right\rangle \in \mathcal{D}^+ \tag{5.4}$$

We can construct a state satisfying these conditions by projecting the perturbed eigenstate onto the original degenerate subspace:

$$\hat{P}_j^+ = \sum_{m=1}^{d_j^+} \left|E_j^+; m\right\rangle\!\left\langle E_j^+; m\right| \tag{5.5}$$

$$\left|E_j^+; P\right\rangle = \hat{P}_j^+ \left|E_i; n\right\rangle = \sum_{m=1}^{d_j^+} \left|E_j^+; m\right\rangle \left\langle E_j^+; m \middle| E_i; n\right\rangle \tag{5.6}$$

Now we can express a general eigenstate of $\hat{H}$ as a superposition of an eigenstate of $\hat{H}^+$ with a norm that goes like $1 - O(\lambda)$ and a remainder. We normalize the components and introduce superposition coefficients:

$$\left|E_i; n\right\rangle = c_{ES} \left|E_j^+; ES\right\rangle + c_R \left|R\right\rangle \tag{5.7}$$

where the *elevated symmetry component* is defined as

$$\left|E_j^+; ES\right\rangle = \left|E_j^+; P\right\rangle \left|\left\langle E_j^+; P \middle| E_j^+; P\right\rangle\right|^{-1/2}$$

$$= \left|E_j^+; P\right\rangle \left(\sum_{m=1}^{d_j^+} \left|\left\langle E_j^+; m \middle| E_i; n\right\rangle\right|^2\right)^{-1/2} \tag{5.8}$$

$$c_{ES} = \left\langle E_j^+; ES \middle| E_i; n\right\rangle$$

$$= \sqrt{\sum_{m=1}^{d_j^+} \left|\left\langle E_j^+; m \middle| E_i; n\right\rangle\right|^2} \tag{5.9}$$

$$\sim 1 - O(\lambda)$$

and the *residual component* then becomes

$$\left|R\right\rangle = c_R^{-1} \left(\left|E_i; n\right\rangle - c_{ES} \left|E_j^+; ES\right\rangle\right) \tag{5.10}$$

By demanding norm 1, we obtain:

$$1 = c_R^{-2} \left(\left\langle E_i; n \middle| E_i; n\right\rangle + c_{ES}^2 \left\langle E_j^+; ES \middle| E_j^+; ES\right\rangle - 2c_{ES} \left\langle E_i; n \middle| E_j^+; ES\right\rangle\right)$$

$$c_R = \sqrt{1 - c_{ES}^2} \tag{5.11}$$

$$\sim O(\lambda)$$

$$\left|R\right\rangle = \left(1 - c_{ES}^2\right)^{-1/2} \left(\left|E_i; n\right\rangle - c_{ES} \left|E_j^+; ES\right\rangle\right) \tag{5.12}$$

5.1.2   Selection rules for the elevated symmetry component

Consider now two eigenstates of $\hat{H}$ at different energy levels, $|E_i; n_i\rangle$, $|E_f; n_f\rangle$. If we perturb the system with an interaction Hamiltonian $\hat{H}'$, the rate of transition between these two states is given by Fermi's golden rule [24, Eq. (3.2)]

$$\Gamma_{|E_i;n_i\rangle \to |E_f;n_f\rangle} = \frac{2\pi}{\hbar} \left| \langle E_f; n_f |\hat{H}'| E_i; n_i \rangle \right|^2 \tag{5.13}$$

Since the energy levels may be degenerate, we must consider a full basis for each of the two energy levels to obtain the full transition rate.

Let the energy levels E_i, E_f be chosen such that the direct product $\Gamma_{r(i)}^{(G)} \otimes \Gamma_{\hat{H}'}^{(G)} \otimes \Gamma_{r(f)}^{(G)}$ contains the identity irrep of G, and hence the matrix elements for energy level basis vectors do not vanish due to the selection rule (Sec. 4.2.1). Let us now decompose the two eigenstates into elevated symmetry and residual components:

$$|E_i; n_i\rangle = c_{ES}^i \left| E_{i'}^+; ES \right\rangle + c_R^i |R_i\rangle \tag{5.14}$$
$$|E_f; n_f\rangle = c_{ES}^f \left| E_{f'}^+; ES \right\rangle + c_R^f |R_f\rangle \tag{5.15}$$

where $E_{i'}^+, E_{f'}^+$ denote the energy levels of the high-symmetry Hamiltonian $\hat{H}^+$ which get perturbed into E_i, E_f respectively.

Let us now calculate the matrix element under the interaction Hamiltonian:

$$\langle E_f; n_f |\hat{H}'| E_i; n_i \rangle =$$
$$\left(c_{ES}^f \right)^* c_{ES}^i \left\langle E_{f'}^+; ES \left| \hat{H}' \right| E_{i'}^+; ES \right\rangle + \left(c_{ES}^f \right)^* c_R^i \left\langle E_{f'}^+; ES \left| \hat{H}' \right| R_i \right\rangle +$$
$$\left(c_R^f \right)^* c_{ES}^i \left\langle R_f \left| \hat{H}' \right| E_{i'}^+; ES \right\rangle + \left(c_R^f \right)^* c_R^i \left\langle R_f |\hat{H}'| R_i \right\rangle \tag{5.16}$$

We know that $\left(c_R^f \right)^* c_R^i$ goes like $O\left(\lambda^2\right)$, and hence we will disregard the corresponding term. There are now two possibilities for what may occur:

1. *The elevated symmetry matrix element does not vanish.* If $\Gamma_{r+(i')}^{(G_+)} \otimes \Gamma_{\hat{H}'}^{(G_+)} \otimes \Gamma_{r+(f')}^{(G_+)}$ contains the identity irrep of G_+, the leading term matrix element does not vanish, and forms the main contribution to the total matrix element.

2. *The elevated symmetry matrix element vanishes.* If $\Gamma_{r+(i')}^{(G_+)} \otimes \Gamma_{\hat{H}'}^{(G_+)} \otimes \Gamma_{r+(f')}^{(G_+)}$ does not contain the identity irrep of G_+, the leading term matrix element vanishes due to the selection rule (since it must transform as a scalar). The only non-zero terms are now the cross-terms, which both go like $O(\lambda)$, and the transition rate goes like $O(\lambda^2)$. Hence, even though these spectral lines are not fully forbidden by the selection rule, they are reduced by an order of magnitude (and vanish in first order) due to their high partial symmetry–this is symmetry suppression.

Because $\hat{H}^+$ describes a smaller structure inscribed into the original structure, the perturbation affects the system around the edge of the QD. Therefore we expect wavefunctions which are localised in the centre of the QD to have a high value of c_{ES} and undergo symmetry elevation, whilst wavefunctions with a significant measure around the QD edges should have a high value of c_R, nullifying the effect of symmetry suppression.

5.2   Localisation of heavy-hole excitons in the bulk

The shape of the exciton wavefunctions in the pyramidal QD is not well-understood, as calculating them is highly non-trivial. However, we can state qualitative arguments providing the justification for our expectation of some excitons being highly localised in the bulk of the QD.

For semiconductors with a band-gap under $5\,\mathrm{eV}$, the excitons are mainly of the Wannier-Mott type, for which the electron-hole orbit radius is inversely proportional to the reduced mass [24, p. 78]:

$$r \propto \mu^{-1} = \frac{1}{m_e^*} + \frac{1}{m_h^*} \tag{5.17}$$

$\mathrm{In}_{0.10}\mathrm{Ga}_{0.90}\mathrm{As}$ has a band-gap of $1.28\,\mathrm{eV}$ and the fermionic effective masses $m_e^* \approx 0.059 m_e$, $m_{lh}^* \approx 0.076 m_e$, and $m_{hh}^* \approx 0.5 m_e$. These values were calculated with the formulas provided by Goldberg and Schmidt in [17, p. 62]. These formulas are stated for $T = 300\,\mathrm{K}$, but we expect neither the band-gap nor the effective masses to vary between $T = 30\,\mathrm{K}$ and $300\,\mathrm{K}$ in an order significant for this qualitative argumentation, as the fact that m_e^* and m_{lh}^* are of the same order of magnitude and m_{hh}^* is larger by an order of magnitude should remain true, as well as $E_g < 5\,\mathrm{eV}$.

From this we see that a light-hole neutral exciton has orbit radius approximately twice the value of that of a heavy-hole neutral exciton, making it more delocalised from the QD centre. Based on the particles-in-a-box model derived in Sec. 4.1.1 for the envelope functions, we will extend this qualitative argument for other exciton complexes, too. As shown by Landau in [29, p. 64], lighter particles penetrate further into the walls of a potential well. We hence conjecture that for two exciton complexes of equal number of electrons and equal charge, the exciton with more heavy holes will be more localised in the QD centre, and the exciton with more light holes will be more likely to probe the structure symmetry.

5.3   Identifying intermediate groups of bulk and structure symmetries

Any transformation which is not a symmetry transformation of the crystal bulk is not a true symmetry transformation of the system [30]. Since every element of the structure symmetry G_s is also an element of the bulk symmetry G_b (a fact which requires a specific orientation of the zincblende lattice), any candidate approximate symmetry G_a has to satisfy

$$G_s \subset G_a \subseteq G_b \tag{5.18}$$

Consulting the group chains in [23, Ch. 9], we see that there is only one group that satisfies this condition, which is the bulk symmetry group T_d itself. Our model of symmetry suppression therefore requires T_d to be the symmetry we elevate to, assuming no prior breaking of the structure symmetry G_s.

In the analysis, we have also included the groups D_{3d}, and O_h as close supergroups of C_{3v}, as well as D_{3h}, the close supergroup of C_{3v} which Karlsson *et al.*

	e, $\left\|j = \frac{1}{2}, j_z = \pm\frac{1}{2}\right\rangle$	h-h, $\left\|j = \frac{3}{2}, j_z = \pm\frac{3}{2}\right\rangle$	lh, $\left\|j = \frac{3}{2}, j_z = \pm\frac{1}{2}\right\rangle$
C_{3v}	$E_{1/2}$	$E_{3/2}$ ($^1E_{3/2} \oplus {}^2E_{3/2}$)	$E_{1/2}$
C_{6v}	$E_{1/2}$	$E_{3/2}$	$E_{1/2}$
D_{3h}	$E_{1/2}$	$E_{3/2}$	$E_{5/2}$
D_{3d}	$E_{1/2,g}$	$E_{3/2,u}$ ($^1E_{3/2,u} \oplus {}^2E_{3/2,u}$)	$E_{1/2,u}$

Table 1: Irreps corresponding to electrons, heavy holes, and light holes, respectively, in several point groups. In the parentheses after an irrep label, its decomposition into conjugate representations is denoted if applicable.

claimed to match their experimental data for symmetry-elevated exciton decays, and which gives equal predictions to C_{6v}, another close supergroup [10, p. 19] .

Note that when making predictions for the bulk symmetry group T_d, at the Γ point the light hole band and heavy hole band become degenerate (Fig. 3) and together they transform as a single four-dimensional irrep of T_d. This means that for groups such as T_d, O_h, or any groups where no splitting between the four $j = 3/2$ states occurs, the predictions at the Γ point do not depend on the occupancy numbers of each type of hole, only their total sum.

Also note that for the groups T_d, O_h, the Cartesian rep transforms according to a single irrep, which means the emitted light will not be polarised. As such, it should be detected in both configurations of the waveplate, as it has both σ and z-polarised components. Furthermore, the lines in the σ polarisation and z polarisation should line up at equal energies, since each pair of lines corresponds to a single transition.

5.4 Predictions and their agreement with experiments

The predictions our model makes are the numbers of different emission lines between two exciton complexes. These lines should in theory be separated by fine-structure energy splitting, however, due to accidental degeneracy, some lines may not be resolvable in the experiment. Therefore, observing a lower number of lines than predicted does not necessarily contradict the assumed symmetry group, and more careful analysis of which lines probe the symmetry is needed to robustly disconfirm it.

5.4.1 Fermion transformation properties in different groups

The groups C_{3v}, C_{6v}, D_{3h}, and D_{3d} undergo splitting of the valence band into heavy holes and light holes at the Γ point, and therefore their exciton complexes are fully characterised by the single-fermion transformation properties. See Table 1 for the associated irreps as labelled by Altmann in [23].

Note that the electron and light-hole labels in D_{3h} are $E_{1/2}$ and $E_{5/2}$, respectively. This is interchanged in the analysis of Karlsson *et al.* [10, p. 14], which does not

	one hole	two holes
T_d	$F_{3/2}$	$A_1 \oplus E \oplus T_2$
O_h	$F_{3/2,u}$	$A_{1g} \oplus E_g \oplus T_{2g}$

Table 2: Transformation properties of one hole and two holes in a single energy level, respectively.

lead to different predictions.

The groups T_d and O_h have the heavy hole and light hole bands degenerate at the Γ point, where all holes transform according to a single irrep. Therefore, for these groups we list the transformation properties of both a single-hole state and a double-hole state, with the triple-hole state transforming equally to the single-hole state and the full energy level transforming according to the identity rep (see Sec. 4.2.4). See Table 2 for the associated irreps in the Altmann convention.

5.4.2 Number of lines for exciton and biexciton decays

We have found that D_{3d} gives equal predictions to C_{3v}, C_{6v} gives equal predictions to D_{3h}, and O_h gives equal predictions to T_d, and hence we omit D_{3d}, C_{6v}, and O_h from further analysis for brevity.

The data from Table 3 is compared to experimental data collected by Mattana, Colavecchi, Juska and Pelucchi, which they shared with us together with their preliminary analysis (see Sec. 3.1). The dataset is to-be published, and will be referred to by the authorial initials MCJP. The authors have conducted correlation measurements to identify specific peaks by their corresponding exciton transition. The experimental and analysis details will be included in their upcoming article.

In the Karlsson *et al.* setup, the light-beam is a laser with a spot size of $1\,\mu$m, power in the range 25–750 nW, and wavelength of 532 nm. The sample was kept at the temperature $10-30$ K, and the spectral resolution of the readings is $110\,\mu$eV [10, p. 2].

In the experimental data, for specific transitions there seems to be variations in the spectrum, as if the QDs split into two sub-populations with different properties. Specifically, for $X_{\bar{1}0}$ and $X_{0\bar{1}}$, MCJP identify two separate characteristic spectra shown in Fig. 7. For one sub-population, the missing of one σ-polarised line for $X_{\bar{1}0}$ as noted by Karlsson *et al.* is reproduced. However, in this sub-population, a resolvable z-polarised peak is measured, contradicting the D_{3h} assumption and suggesting an elevation to the bulk symmetry T_d. The resolvable lines in σ and z polarisation for $X_{0\bar{1}}$, conversely, contradict elevation to T_d, as their energies are inequal. The second sub-population matches neither of the analysed groups, as the number of peaks in both polarisations for $X_{\bar{1}0}$ and σ-polarisation for $X_{0\bar{1}}$ seems to increase.

The negatively charged exciton spectra are shown in Fig. 8. Both hole types feature a single strong line in both σ and z polarisation. For $X_{0\bar{1}}^{-}$, this agrees with the predictions of all analysed groups. For $X_{\bar{1}0}^{-}$, the z-polarised peak seems to probe the bulk symmetry T_d, as z-polarised transitions are forbidden in the structure symmetry. However, Karlsson *et al.* seem to have the z-polarised peak appear faintly, or

| Exciton decay label | | σ-polarised | | | z-polarised | | |
short	full	C_{3v}	D_{3h}	T_d	C_{3v}	D_{3h}	T_d
$X_{\bar{1}0}$	$X_{10} \to$ vac.	2	1	1	0	0	1
$X_{0\bar{1}}$	$X_{01} \to$ vac.	1	1	1	1	1	1
$X_{\bar{2}0}^+$	$X_{20}^+ \to$ h-h	1	1	4	0	0	4
$X_{1\bar{1}}^+$	$X_{11}^+ \to$ h-h	2	2	4	2	2	4
$X_{\bar{1}1}^+$	$X_{11}^+ \to$ l-h	4	3	4	2	1	4
$X_{0\bar{2}}^+$	$X_{02}^+ \to$ l-h	1	1	4	1	1	4
$X_{\bar{1}0}^-$	$X_{10}^- \to$ e	1	1	1	0	0	1
$X_{0\bar{1}}^-$	$X_{01}^- \to$ e	1	1	1	1	1	1
$2X_{\bar{2}0}$	$2X_{20} \to X_{10}$	2	1	6	0	0	6
$2X_{1\bar{1}}$	$2X_{11} \to X_{10}$	4	2	6	4	2	6
$2X_{\bar{1}1}$	$2X_{11} \to X_{01}$	6	3	6	2	1	6
$2X_{0\bar{2}}$	$2X_{02} \to X_{01}$	1	1	6	1	1	6
$2X_{\bar{3}0}^+$	$2X_{30}^+ \to X_{20}^+$	1	1	4	0	0	4
$2X_{2\bar{1}}^+$	$2X_{21}^+ \to X_{20}^+$	1	1	4	1	1	4
$2X_{\bar{2}1}^+$	$2X_{21}^+ \to X_{11}^+$	4	3	4	2	1	4
$2X_{1\bar{2}}^+$	$2X_{12}^+ \to X_{11}^+$	2	2	4	2	2	4
$2X_{\bar{1}2}^+$	$2X_{12}^+ \to X_{02}^+$	1	1	4	0	0	4
$2X_{0\bar{3}}^+$	$2X_{03}^+ \to X_{02}^+$	1	1	4	1	1	4

Table 3: The predicted number of different transitions between exciton complexes for the a priori assumed true group C_{3v}, the elevation supergroup D_{3h} as suggested by Karlsson *et al.*, and the only supergroup which also respects bulk symmetry, T_d. The short label for a decay identifies the initial complex and indicates which hole type recombines with a bar over the occupation number.
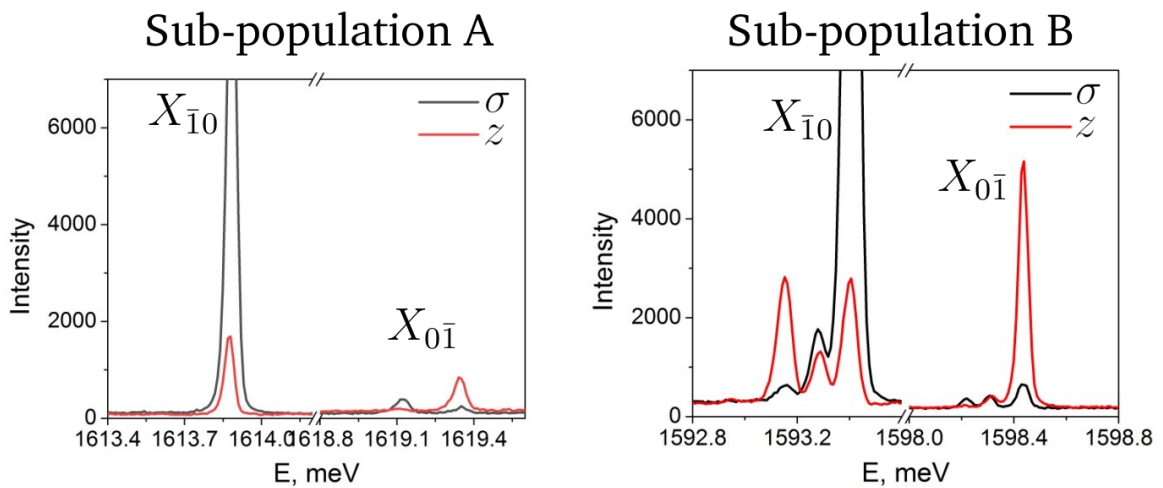
Figure 7: Spectra of two types of QDs in the neutral exciton decays. The σ and z-polarised spectra are colour-coded black and red, respectively.
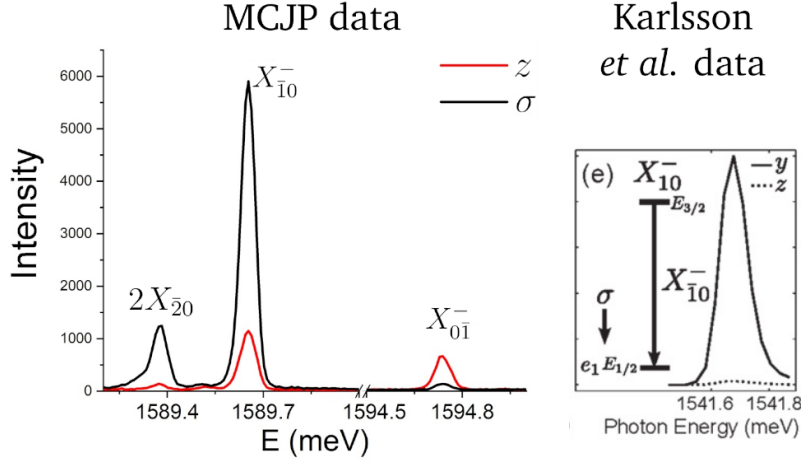
not resolvable at all.

Figure 8: Spectrum of the negatively charged excitons, compared between the new MCJP dataset and the Karlsson dataset. Karlsson dataset plot taken from [10, Fig. 15 e)]

The spectra of positively charged excitons and biexcitons are shown in Fig. 9. For $2X_{\bar{2}1}^{+}$, 3 resolvable peaks with both σ and z-polarised components are always present, with the latter polarisation contradicting the predictions of C_{3v} and D_{3h}. In sub-population A a fourth peak, with both σ and z-polarised components, is usually present, but is not conclusively proven to be part of the complex by the MCJP correlation measurements. 4 peaks in both polarisations would be good evidence for elevating to bulk symmetry.

For $X_{\bar{1}1}^{+}$, three peaks are always certain in both sub-populations, with z-polarised components seemingly weakened and multiple added faint σ-polarised peaks occuring in B. The three z-polarised peaks contradict C_{3v} and D_{3h} predictions and are consistent with T_d for sub-population A, while the 4 σ-polarised and 2 resolvable z-polarised lines show agreement with C_{3v} for sub-population B.

For $X_{1\bar{1}}^{+}$, four strong lines with both σ and z components are present for both types, contradicting C_{3v} and D_{3h} and agreeing with T_d. However, the relative intensities of the lines disconfirm the assumption of emissions with no polarisation, since that predicts components of all polarisations to be of equal relative intensity. Both populations here exhibit the dominance of the z-polarised component for lines c and b. Altogether, this constitues weak evidence for elevation to the bulk symmetry, conditioned by the presence of another mechanism which introduces z-polarisation bias for lines c, b. Interestingly, in the Karlsson *et al.* data, only two lines are detected in either polarisation, in agreement with both C_{3v} and D_{3h}, contradicting the bulk symmetry elevation, for a subpopulation of 15% of their QDs. Other QDs exhibited different spectra, typically with extra lines [10, Fig. 19], which suggest partial elevation to T_d.
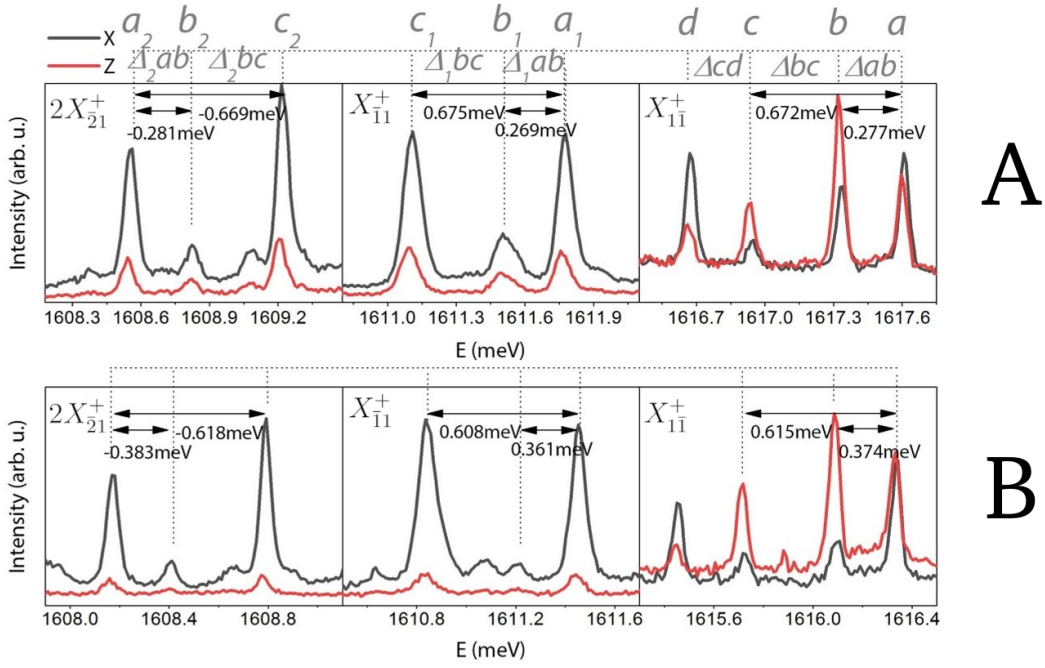
Figure 9: Spectrum of the positive biexciton $2X_{\bar{2}1}^{+}$ and the positive mixed-hole excitons $X_{\bar{1}1}^{+}$ and $X_{1\bar{1}}^{+}$. Two distinct sub-populations were identified, labelled A and B. Major peaks are identified by MCJP and their energy differences highlighted.

For other positively charged excitons and biexcitons, MCJP have no data. However, Karlsson *et al.* identified a single line for either polarisation for $2X_{2\bar{1}}^{+}$, in agreement with C_{3v} and disagreement with T_d. Similarly, $2X_{1\bar{2}}^{+}$ had two σ-polarised lines and one z-polarised line, with another one suggested to be present but unresolvable, in agreement with C_{3v}. For $X_{\bar{2}0}^{+}$, a single σ-polarised line was detected, seemingly in agreement with C_{3v}. However, activity in the z-polarised spectrum is faintly evident. Better-resolved measurement of the z-polarised spectrum may find evidence for weak elevation to the bulk symmetry.

The spectra of neutral biexcitons are shown in Fig. 10. MCJP were unable to conclusively confirm all peaks in the $2X_{\bar{1}1}$ spectrum to belong to it. Due to the ambiguous identification of lines and the unresolvability of the predicted large number of lines, the transition was not analysed here. Karlsson *et al.* note that the z-polarised peaks may be present but very weak due to the heavy-hole recombination [10, p. 16], and thus missing z-polarised lines do not constitute evidence against elevation to T_d.

For the transition $2X_{\bar{2}0}$, a strongly resolvable z-polarised peak is measured, contradicting C_{3v} and D_{3h}. While T_d predicts 6 z-polarised peaks, it is possible that they are too tightly spaced to be resolvable, especially since the energy splitting may be reduced due to the approximate nature of elevating to the bulk within symmetry suppression theory. The Karlsson data does not measure the z-polarised line, which instead suggests elevation to D_{3h}, but that is forbidden by the lattice symmetry.
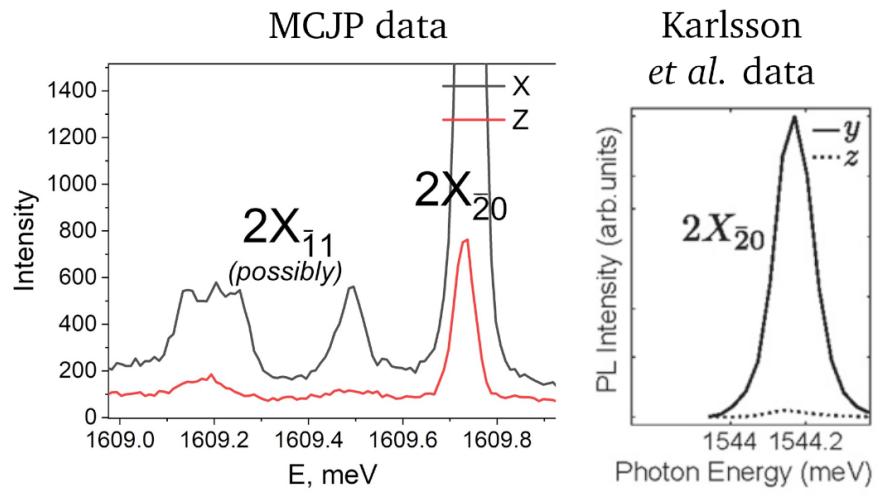
Figure 10: Spectrum of two neutral biexcitons. Karlsson dataset plot taken from [10, Fig. 15 a)]

6 Discussion of results

6.1 Agreement with the bulk symmetry T_d

Observing which exciton complexes seem to elevate to T_d generates predictions within our theory about the localisation of their wavefunctions within the QD bulk. The exciton transitions which were observed to undergo symmetry elevation to T_d in the MCJP dataset are $X_{\bar{1}0}$ (for one sub-population), $X_{\bar{1}0}^-$ (not in the Karlsson data), $2X_{\bar{2}1}^+$ (with one peak being ambiguously identified to the transition), $X_{\bar{1}1}^+$ (for one sub-population), $X_{1\bar{1}}^+$ (with the relative intensity of the polarisations not explicable with symmetry arguments), and $2X_{\bar{2}0}$ (assuming the 6 lines are unresolvable due to tight spacing). Conversely, the excitons $X_{0\bar{1}}$ (for one sub-population), $X_{\bar{1}1}^+$ (for one sub-population), and $X_{1\bar{1}}^+$ (only in the Karlsson data) seem to explicitly disconfirm T_d symmetry and probe for the structure symmetry. It is important to note that the sub-population divisions for the neutral excitons and for the positive excitons are different.

It should be noted that transitions for all other exciton complexes measured by Karlsson *et al.* agree with the structure symmetry C_{3v} [10, p. 20].

The claim in Sec. 5.2 is disproven by the transition $X_{\bar{2}0}^+$, which, per Karlsson *et al.*, obeys the structure symmetry, unlike positive excitons with one heavy and one light hole. However, the other exciton complexes with only heavy holes and 1 or 2 electrons seem to elevate to the bulk symmetry, hence the exciton localisation may still be the factor determining elevation towards the bulk symmetry, if the delocalisation of $X_{\bar{2}0}^+$ can be justified with a more precise model.

The ambiguity for mixed-hole excitons suggests that light holes indeed may, in general, probe the structure symmetry due to their delocalisation. Neither MCJP not Karlsson *et al.* were able to resolve the light hole-dominant excitons for which the predictions of C_{3v} and T_d differ ($X_{0\bar{2}}^+$, $2X_{0\bar{2}}$, and positive biexcitons with 2 or 3 light holes). Resolving these transitions is important material for further study, since if they behave according to structure symmetry, it would be evidence that the symmetry suppression model correctly identifies the mechanism for symmetry elevation.

Regarding the transition $X_{1\bar{1}}^+$ (Fig. 9), Karlsson *et al.* have experimentally measured the fine-strucure energy splitting of the exciton complex X_{11}^+, ordering its corresponding energy levels labelled by their transformation properties [10, p. 16]. In C_{3v}, the lowest and highest energy levels transform as $E_{3/2}$, and the middle two energy levels transform as $E_{1/2}$ [10, Fig. 17]. This could explain the relative intensities of differently-polarised components of lines in the MCJP dataset, with the z-polarisation dominance in lines c, b caused by the different transformation properties of their initial states compared to the initial states of lines d, a. It is possible that the wavefunction centre-localisation depends on the exciton transformation properties, affecting the magnitude of symmetry suppression enjoyed by specific lines.

6.2 Possible sources of error from theoretical treatment and experimental setup

In our treatment of the exciton envelope functions, we disregard band-mixing effects caused by the nanocrystal structure and small number of lattice points (Sec. 4.1.1). However, the pyramidal QDs subject to this study exhibit strong valence band mixing, which affects photoluminiscence polarisation [31]. This may affect the envelope function treatment, especially outside of the Γ point, as it contradicts an assumption in the treatment. However, the effect the valence-band mixing has on photoluminiscence polarisation may also aid in explaining the relative intensities of the differently-polarised lines. A more mathematically robust treatment of envelope functions is crucial material for further study.

An important phenomenon disregarded in our treatment is the effect of structure interfaces, which affect the Hamiltonian symmetry group [32]. Whilst a full treatment of the symmetry suppression model has to address this to prove elevation to T_d is still possible, this could also validate our data e.g. by providing the polarisation bias to $X_{1\bar{1}}^+$, explaining the relative line intensities.

Finally, for all transitions where we identify elevation to T_d, the main evidence consists of the increased number of z-polarised lines from the one predicted by C_{3v} and D_{3h}. Hence our argumentation relies on the fact that these z-polarised components were identified correctly. However, if a physical effect unaccounted for in the experimental setup caused the reading of a non-zero z-polarised component where the emission has no z-polarised component, the measured z-polarised line would match the frequency of the measured σ-polarised line, analogously to how the non-polarised light predicted by T_d produces lines of matching frequencies in both polarisations. This alternative explanation is supported by the apparent partial disagreement between the MCJP and Karlsson *et al.* datasets specifically regarding the presence of z-polarised lines (Fig. 8, 10). In future study, careful reproduction of the z-polarised spectra for exciton complexes identified as elevating to bulk symmetry is crucial for disproving the symmetry suppression hypothesis.

6.3 Insufficient treatment of line number increase

The model of symmetry suppression postulates that excitons with wavefunctions localised in the QD bulk enjoy approximate elevation to the bulk (lattice symmetry). Within this model, lines which are light in the lower symmetry but dark in the elevated symmetry will be heavily suppressed. However, the opposite effect (where the number of lines increases with symmetry elevation), which occurs for certain excitons when elevating to T_d, is non-trivial. This is because the increase of number of lines is often caused by the change of transformation properties of holes when the light hole band and heavy hole band become degenerate at Γ (Table 2). Within symmetry suppression theory, we consider the component of a low-symmetry eigenstate which forms an eigenstate of a high-symmetry Hamiltonian, but the residual component still demands different energy levels for the two hole types, suppressing the band distance but keeping it non-zero. For the model to be rigorous, additional treatment of this phenomenon must be introduced, either resolving the transforma-

tion properties of holes under elevation to a group with the hole bands degenerate, or by identifying a mechanism that couples the different-character holes together, salvaging the degenerate behaviour within our model. This is material for further study of symmetry elevation within the symmetry suppression framework.

6.4 Symmetry outside of the Γ point

In the symmetry suppression model, we have assumed all excited fermions to have zero crystal momentum, which is necessary to use the "charged particles in a box" dynamics for the envelope functions. However, this is only an approximation based on the nature of the direct band-gap of InGaAs. For an excited fermion outside of the Γ point in a large crystal, the non-zero crystal momentum vector $\vec{k}$ breaks the wavefunction symmetry, as described by Dresselhaus in [22, Ch. 13]. In an interplay with the bulk symmetry, the true symmetry of the Hamiltonian $\hat{H}\left(\vec{k}\right)$ depends on the crystal momentum.

In our nanocrystal, the effects of the crystal size alter the band structure, and a full description of the wavefunction is not possible with the crystal momentum, but rather with the shape of the envelope function, which is poorly understood. Exciting the envelope function from the ground state (i.e. leaving the Γ point) may break some symmetries, but in general, it also changes the transformation properties of the wavefunction, since $\chi^{(\Upsilon(\vec{r}))}\left(\hat{R}\right)$ in Eq. (4.22) is no longer always unity. This could potentially explain the division of QDs into two sub-populations for some exciton complexes (and the discrepancy with the Karlsson data), where the distribution of envelope function energies would become a non-trivial statistical phenomenon. However, the shapes of the envelope functions are not yet well understood, as they are highly sensitive to high-order or mechanical effects, such as strain-induced piezo-electricity (Fig. 11).

Of course, since the extra degree of freedom in transformation properties could alter any prediction for photoluminiscence spectrum, it may also serve as an alternative explanation to symmetry elevation.
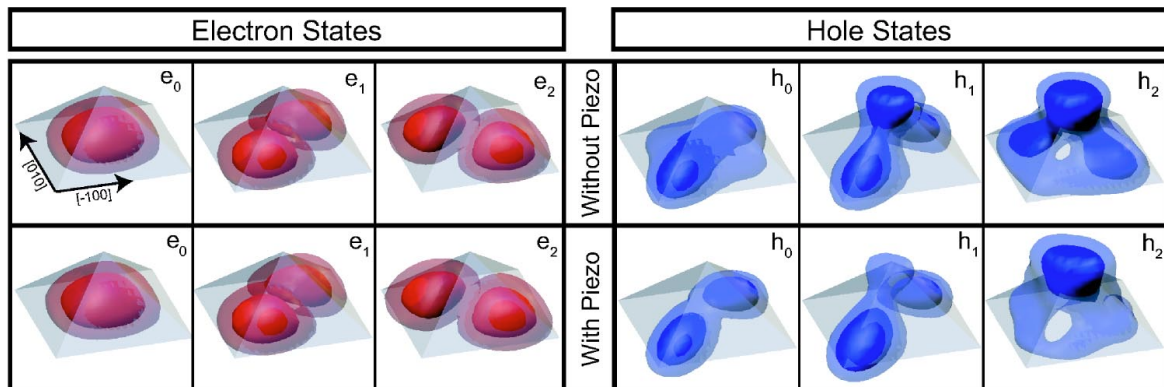

Figure 11: Envelope functions of ground- and excited-state electrons and holes in a C_{4v} pyramid structure for first-order theory and including strain-induced piezoelectric effect. Figure taken from [30, Fig. 6]

7 Conclusions

Based on the arguments in [30] and our analysis of the zincblende lattice of InGaAs quantum dots, we claim that neither of the symmetry groups proposed by Karlsson *et al.* (D_{3h}, C_{6v}) can be the symmetry group of the Hamiltonian under symmetry elevation. In our model, where the extra symmetries are provided by the atomic lattice in the nanocrystal bulk, we have outlined a general condition for a possible elevated-symmetry group given by the true symmetry and the bulk symmetry (Eq. (5.18)). In general, the true symmetry group G_s may be lower than the structure symmetry due to mismatching orientation of rotations for structure symmetries and bulk symmetries.

Applying this method, we have identified T_d as the only candidate group which C_{3v} can elevate to. Comparing the predictions for emission spectra arising from this group to the to-be published MCJP data, we find partial agreement, suggesting certain excitons undergoing elevation to T_d for at least a certain fraction of the grown QDs.

The true symmetry of the Hamiltonian may be a different subgroup of T_d if prior symmetry breaking occurs in the system, e.g. due to interface effects, piezo-electric or other strain-induced effects, excited-state envelope functions, or other untreated physical phenomenons. Testing the predictions given by subgroups of T_d which do not contain C_{3v} is material for further study, as finding agreement with such a group can also provide clues about the nature of symmetry breaking in the system.

We have constructed a theoretical model of symmetry suppression in Sec. 5.1 as a proposed mechanism for elevating towards bulk symmetry. The model suffices to explain the approximate darkening (suppression) of emission lines as identified by Karlsson *et al.*, but fails to justify the raised degeneracy of valence bands at Γ which is required to reach T_d symmetry (Sec. 6.3). A more robust treatment, possibly incorporating higher-order effects and band-mixing effects is needed to justify this corollary of symmetry elevation to T_d.

Within the model of symmetry suppression, excitons are more likely to elevate to bulk symmetry if more of their holes are heavy-like. We conclude that this is untrue for positively charged excitons, but holds for all other exciton and biexciton complexes, hinting at a mechanism affecting wavefunction localisations which is untreated in our simplistic model in Sec. 5.2. The exciton transitions $X_{0\bar{2}}^+, 2X_{0\bar{2}}^+, 2X_{\bar{1}2}^+, 2X_{1\bar{2}}^+, 2X_{0\bar{3}}^+$ were not yet experimentally resolved, and if future studies demonstrate these transitions to behave according to the structure symmetry, it would both provide evidence that symmetry suppression is the mechanism for symmetry elevation and predict within the model that the associated exciton complexes are not localised in the centre of the quantum dot.

As demonstrated by the discrepancies between the MCJP and Karlsson datasets, as well as the different behaviours of distinct QDs within each dataset, the features of the photoluminiscence spectra of these structures cannot be reliably predicted only by arguments based on the structure and bulk symmetry properties. While a good stepping stone, a fuller understanding of both the symmetry of the true Hamiltonian and other effects which may affect the photoluminiscence spectrum is needed.

8   Acknowledgements

9 Bibliography

[1] Michler, P. (2017), *Quantum Dots for Quantum Information Technologies*. 1st edn. Springer Cham. doi.org/10.1007/978-3-319-56378-7

[2] Juska, G. *et al.* (2016), A Site-Controlled Quantum Dot Light-Emitting Diode of Polarization-Entangled Photons, Violating Bell's Inequality. *CLEO: QELS_Fundamental Science 2016* (conference). Available at opg.optica.org/abstract.cfm?uri=CLEO_QELS-2016-FTu1C.2

[3] Jin, X. *et al.* (2020), Cation exchange assisted synthesis of ZnCdSe/ZnSe quantum dots with narrow emission line widths and near-unity photoluminescence quantum yields. *Chem. Commun.*, **56** (45), 6130–6133. doi.org/10.1039/D0CC01302A

[4] Hanifi, D. A. *et al.* (2019), Redefining near-unity luminescence in quantum dots with photothermal threshold quantum yield. *Science*, **363** (6432), 1199–1202. doi.org/10.1126/science.aat3803

[5] Medintz, I. L. *et al.* (2005), Quantum dot bioconjugates for imaging, labelling and sensing. *Nature Mater.*, **4**, 435–446. doi.org/10.1038/nmat1390

[6] Sakimoto, K. K., Wong, A. B., Yang, P. (2016), Self-photosensitization of non-photosynthetic bacteria for solar-to-chemical production. *Science*, **351** (6268), 74–77. doi.org/10.1126/science.aad3317

[7] García de Arquer, F. P. *et al.* (2021), Semiconductor quantum dots: Technological progress and future challenges. *Science*, **373** (6555). doi.org/10.1126/science.aaz8541

[8] Ashoori, R. C. (1996), Electrons in artificial atoms. *Nature*, **379**, 413–419. doi.org/10.1038/379413a0

[9] Cho, A. Y., Arthur, J. R. (1975), Molecular beam epitaxy. *Progress in Solid State Chemistry*, **10** (3), 157–191. doi.org/10.1016/0079-6786(75)90005-9

[10] Karlsson, K. F. *et al.* (2015), Spectral signatures of high-symmetry quantum dots and effects of symmetry breaking. *New J. Phys.*, **17**, 103017. doi.org/10.1088/1367-2630/17/10/103017

[11] Hartmann, A. *et al.* (2000), Few-Particle Effects in Semiconductor Quantum Dots: Observation of Multicharged Excitons. *Phys. Rev. Lett.*, **84** (24), 5648–5651. doi.org/10.1103/PhysRevLett.84.5648

[12] Wightman, A. S. (1995), Eugene Paul Wigner 1902–1995. *Notices Amer. Math. Soc.*, **42** (7), 769-771. Available at www.ams.org/notices/199507/wigner.pdf

[13] Karlsson, K. F. *et al.* (2010), Fine structure of exciton complexes in high-symmetry quantum dots: Effects of symmetry breaking and symmetry elevation. *Phys. Rev. B*, **81** (16), 161307(R). doi.org/10.1103/PhysRevB.81.161307

[14] Dupertuis, M. A. *et al.* (2011), Symmetries and the Polarized Optical Spectra of Exciton Complexes in Quantum Dots. *Phys. Rev. Lett.*, **107** (12), 127403. doi.org/10.1103/PhysRevLett.107.127403

[15] Hartmann, A. *et al.* (1997), Self-limiting growth of quantum dot heterostructures on nonplanar $\{111\}B$ substrates. *Appl. Phys. Lett.*, **71** (10), 1314–1316. doi.org/10.1063/1.119882

[16] Holsgrove, K. M., O'Reilly, T. I., Varo, S. *et al.* (2022), Towards 3D characterisation of site-controlled InGaAs pyramidal QDs at the nanoscale. *J Mater Sci*, **57** 16383–16396. doi.org/10.1007/s10853-022-07654-2

[17] Goldberg, Y. A., Schmidt, N. M. (1996), *Gallium Indium Arsenide ($Ga_xIn_{1-x}As$)* in *Handbook Series on Semiconductor Parameters: Volume 2: Ternary And Quaternary III-V Compounds* (edited by Levinshtein, M., Rumyantsev, S., Shur, M.). World Scientific, London. ISBN 981-02-1420-0 (Set)

[18] Singh, J. (2003), *Electronic and Optoelectronic Properties of Semiconductor Structures* (1st ed.). Cambridge University Press, Cambridge. doi.org/10.1017/CBO9780511805745

[19] Burt, M. G. (1999), Fundamentals of envelope function theory for electronic states and photonic modes in nanostructures. *J. Phys.: Condens. Matter*, **11** (9), 53. doi.org/10.1088/0953-8984/11/9/002

[20] Dresselhaus, M. S., Dresselhaus, G., Jorio, A. (2007), *Group Theory: Application to the Physics of Condensed Matter* (1st ed.). Springer Berlin, Heidelberg. doi.org/10.1007/978-3-540-32899-5

[21] Burt, M. G. (1992), The justification for applying the effective-mass approximation to microstructures. *J. Phys.: Condens. Matter*, **4** (32), 6651–6690. doi.org/10.1088/0953-8984/4/32/003

[22] Dresselhaus, M. S. (2002), *Applications of Group Theory to the Physics of Solids*. Massachusetts Institute of Technology (unpublished). Available at web.mit.edu/course/6/6.734j/www/group-full02.pdf

[23] Altmann, S. L., Herzig, P. (1994), *Point-Group Theory Tables*. Clarendon Press, Oxford. ISBN 0-19-855226-2

[24] Fox, M. (2002), *Optical Properties of Solids (Oxford Master Series in Physics)* (1st ed.). Oxford University Press. ISBN 0-19-850613-9

[25] Parmenter, R. H. (1955), Symmetry Properties of the Energy Bands of the Zinc Blende Structure. *Phys. Rev.*, **100** (2), 573–579. doi.org/10.1103/PhysRev.100.573

[26] Wigner, E. P. (1959), *Group Theory and Its Application to the Quantum Mechanics of Atomic Spectra* (transl. by Griffin, J. J.) (Expanded and improved ed.). Academic Press, New York and London. Library of Congress Catalog Card No. 59-10741 (Original work published in 1951)

[27] Hsiaw, H. C. *et al.* (1988), Valence and conduction band molecular-orbital topologies and the optical and electrical properties of gallium arsenide and silicon. *J. Non-Cryst. Solids,* **105** (1–2), 101–106. doi.org/10.1016/0022-3093(88)90343-2

[28] Tournet, J. (2015), *Growth and Characterization of Epitaxial Al Layers on GaAs and Si Substrates for Superconducting CPW Resonators in Scalable Quantum Computing Systems* (MASc thesis, University of Waterloo). Waterloo, Ontario. Available at core.ac.uk/download/pdf/144148499.pdf

[29] Landau, L. D., Lifshitz, E. M. (1977, repr. 1991 w. corrections), *Quantum Mechanics: Non-Relativistic Theory* (transl. by Sykes, J. B., Bell, J. S.) (3rd ed., revised a. enlarged). Pergamon Press, Oxford. ISBN 0-08-020940-8 (Translated from 4th ed. published in 1989)

[30] Bester, G., Zunger, A. (2005), Cylindrically shaped zinc-blende semiconductor quantum dots do not have cylindrical symmetry: Atomistic symmetry, atomic relaxation, and piezoelectric effects. *Phys. Rev. B,* **71** (4), 045318. doi.org/10.1103/PhysRevB.71.045318

[31] Zhu, Q. *et al.* (2007), Transition from two-dimensional to three-dimensional quantum confinement in semiconductor quantum wires/quantum dots. *Nano Lett.,* **7** (8), 2227–33. doi.org/10.1021/nl0706650

[32] Tomić, S., Vukmirović, N. (2011), Symmetry reduction in multiband Hamiltonians for semiconductor quantum dots: The role of interfaces and higher energy bands. *J. Appl. Phys.,* **110** (5), 053710. doi.org/10.1063/1.3631048